

High Throughput Phenotyping of Cross-sectional Morphology in Plant Stalks: Sample Preparation,
Image Processing, and Feature Extraction

A Thesis

Presented in Partial Fulfillment of the Requirements for the

Degree of Master of Science

with a

Major in Mechanical Engineering

in the

College of Graduate Studies

University of Idaho

by

Yusuf Abiodun Oduntan

Major Professor: Daniel Robertson, Ph.D.

Committee Members: Steven Beyerlein, Ph.D.; Gabriel Potirniche, Ph.D.

Department Administrator: Gabriel Potirniche, Ph.D.

May 2021

Authorization to Submit Thesis

This thesis of Yusuf Abiodun Oduntan, submitted for the degree of Master of Science with a Major in Mechanical Engineering and titled ‘High Throughput Phenotyping of Cross-sectional Morphology in Plant Stalks: Sample Preparation, Image Processing, and Feature Extraction,’ has been reviewed in final form. Permission, as indicated by the signatures and dates below, is now granted to submit final copies to the College of Graduate Studies for approval.

Major Professor: _____ Date: _____

Daniel Robertson, Ph.D.

Committee Members: _____ Date: _____

Steven Beyerlein, Ph.D.

_____ Date: _____

Gabriel Potirniche, Ph.D.

Department

Administrator: _____ Date: _____

Gabriel Potirniche, Ph.D.

Abstract

Stalk lodging (mechanical failure of plant stalks during windstorms) leads to global yield losses in cereal crops estimated to range from 5-25% annually. The cross-sectional morphology of plant stalks is a key determinant of stalk lodging resistance. However, previously developed techniques for quantifying cross-sectional morphology of plant stalks are low-throughput, expensive and require specialized equipment and expertise. There is need for a simple and cost-effective techniques to quantify plant traits related to stalk lodging resistance in a high-throughput manner.

To this end a rapid, low-cost, and user-friendly phenotyping methodology was developed to quantify two-dimensional plant cross sections. The methodology offers reduced sample preparation time and cost as compared to previously developed techniques. The new methodology employs an inexpensive stereoscope and a semi-automated image processing algorithm. The algorithm can be used to produce specimen specific, dimensionally accurate computational models (including finite element models) of plant stalks.

This new methodology was applied to a range of plant samples including, maize (*Zea mays*), sorghum (*Sorghum bicolor*), wheat (*Triticum aestivum*), poison hemlock (*Conium maculatum*), and Arabidopsis (*Arabis thaliana*). The major diameter, minor diameter, rind thickness and number of vascular bundles were quantified for each of these plant types. Linear correlation analyses demonstrated strong agreement between the newly developed method and more time-consuming manual techniques ($R^2 > 0.9$). In addition, the new method was used to generate several specimen specific finite element models of plant stalks. All of the models compiled without issue and were successfully imported into finite element software. All the models demonstrated reasonable and stable solutions when subjected to realistic applied loads.

Acknowledgments

I wish to express my deepest appreciation to Dr. Daniel Robertson, for his guidance, assistance, understanding, patience, and freedom to work throughout the duration of my program.

I would like to thank Dr. Christopher Stubbs for his outstanding and invaluable support, assistance, and advice during my program and at every step of this project.

I would like to appreciate the instrumental contributions and support of Dr. Gabriel Potirniche and Dr. Steven Beyerlein to developing and completing this project.

I would like to thank Daniel Mottern for his instrumental assistance and advice in developing staining and imaging techniques.

I would like to thank the department of mechanical engineering for their institutional support.

I would like to thank the Global Student Support Program (GSSP) staff for their support and guidance, particularly in helping me integrate seamlessly into the school environment.

Table of Contents

Authorization to Submit Thesis	ii
Abstract.....	iii
Acknowledgments	iv
Table of Contents.....	v
List of Tables	vii
List of Figures	viii
Chapter 1: Introduction	1
1.1 Plant Biomechanics.....	1
1.2 Crop Stalk Lodging	3
1.3 Plant Anatomy	4
1.4 Problem Statement.....	7
Chapter 2: Literature Review.....	8
2.1 Sample Preparation	8
2.2 Imaging	10
2.3 Feature Extraction	13
Chapter 3: Sample preparation	15
3.1 Samples.....	15
3.2 Sample Sectioning.....	16
3.3 Sample Sectioning Results	17
3.4 Recommended Practices for Sectioning	19
Chapter 4: Image Analysis	20
4.1 Specimen Staining.....	20
4.2 Recommended Practices for Specimen Staining	20
4.3 Imaging	23

4.4 Recommended Practices for Imaging	23
4.5 Recommended Practices for Image Analysis	24
Chapter 5: Feature Extraction.....	25
5.1.1 Pre-processing	25
5.1.2 Segmentation.....	25
5.1.3 Smoothing Operations.....	25
5.1.4 Quantification	26
5.2 Feature Extraction Results	26
5.3 Comparisons Among Plant Samples	31
Chapter 6: Exporting Extracted Plant Features to Third Party Software	34
6.1 Geometry Importation.....	34
6.2 Computer Modeling.....	36
Chapter 7: Conclusions, Recommendations, and Future Work	42
7.1 Conclusion.....	42
7.2 Recommendations	42
7.3 Future Work	43
References	44
Appendix A: Protocol for Phenotyping Maize or Sorghum Stalks	50
Appendix B: Protocol for Phenotyping Poison Hemlock Stalks	52
Appendix C: Protocol for Phenotyping Wheat and Arabidopsis Stalks	54
Appendix D: MATLAB Code for the Image Processing of Maize and Sorghum Stalks.	56
Appendix E: MATLAB Code for the Image Processing of Wheat, Poison Hemlock and Arabidopsis Stalks.....	63

List of Tables

Table 3.1: Plant Types and Descriptions	15
Table 3.2: Evaluation of Cutting Machines for Plant Sectioning	18

List of Figures

Figure 1.1: How Plant Phenotypes are Formed [6].....	2
Figure 1.2: Stalk Lodging in Maize [11].	4
Figure 1.3: Safranin O and Alcian Blue Stained Cross-section of maize (left) and wheat (right) showing their tissue types.	6
Figure 1.4: Typical profile of cereal crop stalks [13].	6
Figure 2.1: Workflow for Plant Phenotyping.	8
Figure 2.2: A vibratome (Leica VT 1200S) [24] (left) and a microtome (Leica RM2245) [25] (right).	10
Figure 2.3: A Scanning Electron Microscope (SEM) (JEOL JSM-7610F) showing its electron beam generator column, specimen chamber, vacuum pump, monitor, and control panels [32].	11
Figure 2.4: A Computed Tomography (CT) Scanner (GE Phoenix Nanotom System) showing its specimen cabinet [33].	12
Figure 2.5: A Magnetic Resonance Imaging (MRI) Scanner (Bruker Biospec Scanner) showing its specimen Chamber [34].	12
Figure 3.1: Phenotypes Extracted and Measurements Taken for Maize (left), and wheat (right).	16
Figure 3.2: Machine set-ups for sectioning samples. Set-up of Metabo WEV15-125 Angle Grinder (left), Set-up of Hi-Tech Diamond 6” Trim Saw (center) and Set-up of Makita 2414DB Cut-Off Saw (right).	17
Figure 3.3: Problems encountered while sectioning; A) Burnt/stained section surfaces, B) sections with ripped rinds, C) Sections with pulled vascular bundles D) oblique section surfaces.	18
Figure 4.1: Plant sections of A) Maize and B) Sorghum stained with i) Safranin O, ii) Toluidine Blue and iii) Alcian Blue.	21
Figure 4.2: Plant sections of A) Poison Hemlock, B) Wheat, C) Arabidopsis stained with i) Safranin O, ii) Toluidine Blue and iii) Alcian Blue.....	21
Figure 4.3: Alcian Blue-Safranin O Staining Sequence.....	22
Figure 4.4: A) Maize, B) Sorghum, C) Poison Hemlock, D) Wheat and E) Arabidopsis samples stained using the Safranin O-Alcian Blue Staining Sequence.	22
Figure 4.5: Image of stained section obtained using a flatbed scanner (hp LaserJet)	23
Figure 4.6: 3.5X-180X Trinocular Stereo Microscope with 18 MP Camera (left) and Barlow lenses 0.5X (middle) for wide field of view and 2X (right) for better magnification.	24

Figure 5.1: Raw (RGB) image and thresholded (binarized) image of maize (left) and wheat (right) sections	27
Figure 5.2: Segmented areas: i) maize whole cross-sectional area ii) maize pith area iii) wheat whole cross-sectional area iv) wheat hollow area.	27
Figure 5.3: Smoothed images of i) maize whole cross-sectional area, ii) maize pith area, iii) vascular bundles within maize pith and iv) wheat whole cross-sectional area.....	27
Figure 5.4: Maize section (left) and wheat section (right) showing extracted rind boundaries, major and minor diameter lines, rind thickness measurement lines and maize vascular bundle boundaries (left).	28
Figure 5.5: A maize section's automatically identified vascular bundles (left) and its grayscale image with overlaid identified vascular bundle boundaries and plotted circles for manually selected vascular bundles (right).	28
Figure 5.6: Measured vs calculated major diameter measurements of wheat, sorghum, maize, and poison hemlock.....	29
Figure 5.7: Measured vs calculated minor diameter measurements of wheat, sorghum, maize, and poison hemlock.....	30
Figure 5.8: Measured vs calculated rind thickness measurement of wheat, sorghum, maize, and poison hemlock.....	30
Figure 5.9: Manually Identified vs Automatically identified vascular bundles from maize and sorghum piths.	31
Figure 5.10: Quantification of phenotypes obtained for maize varieties using image analysis algorithm	32
Figure 5.11: Quantification of phenotypes obtained for sorghum varieties using image analysis algorithm	33
Figure 6.1: Pseudo code used to import geometry into third party software.	35
Figure 6.2: Imported maize stem specimen specific cross-sectional geometry.....	36
Figure 6.3: Undeformed (left) and Deformed (right) models of a maize stalk loaded in compression, showing Von Mises stress (MPa) experienced from the top internode (top) to the bottom internode (bottom).....	38
Figure 6.4: Undeformed three-dimensional model of maize stalk (right) and its cross-section (left). .	39
Figure 6.5: Undeformed three-dimensional model of wheat stalk (right) and its cross-section (left). .	39
Figure 6.6: Boundary conditions and loads applied to maize stalk model.	40

Figure 6.7: Boundary conditions and loads applied to wheat stalk model.	40
Figure 6.8: Deformed model of maize stalk internode under bending showing principal stress (MPa) contours along the stalk.	41
Figure 6.9: Deformed model of wheat stalk internode under bending showing principal stress (MPa) contours along the stalk.	41

Chapter 1: Introduction

1.1 Plant Biomechanics

Plant life accounts for over 90% of all visible living matter, they absorb carbon dioxide, release oxygen, regulate the water cycle, serve as model organisms for genetic studies, and provide food, habitat and medicine for animals and humans [1]. Consequently, many facets of plant life have been studied over the years. These traditional plant studies have produced greater understanding of genetic networks, subcellular processes, biochemical pathways and more. However, to fully understand plant life, it is essential to investigate how physical and mechanical forces and processes influence plant growth, performance, and evolution [1,2]. This is the focus of the field of plant biomechanics.

The study of plant biomechanics has led to progress in numerous fields of scientific inquiry. Historically, mathematicians, physicists and engineers have gained great insights by collaborating with plant scientists. For example, plants have been used as models to illustrate physical principles and construct mechanical devices. Galileo Galilei used hollow plant stalks to illustrate the importance of outer boundary materials in resisting bending forces, Leonardo da Vinci gained interest in fluid mechanics due to his observation that the cross-sectional areas of tree trunks are roughly equal to the sum of the cross-sectional areas of branches above any point along a trunk's length. The dimensionless equation developed by Osborne Reynolds which enables the modeling of fluid flow around objects has greatly influenced the bio-fluid mechanics field [1,3]. One of the first detailed plant biomechanics publications was by Simon Schwendener in 1874. In his work he applied fundamental engineering concepts to his research on the functional anatomy and morphology of plants [3,4]. His publication introduced several tools and concepts including: a plant's mechanical-ecological relationship, analyzing a plant's habitat and experienced stresses, a plant's composition of composite materials and the anatomical construction of plant tissues.

The quantification of "*Plant Phenotypes*" is an essential part of plant biomechanics. Plant phenotypes are physical plant features or traits that result from interactions between a plant's genotype and its environment. In other words, a plant's "Genotype" represents the genetic blueprint (DNA) of the plant. Whereas a plant's "Phenotype" represents the physical expression of that Genotype in a given environment. Plants are subjected to various biotic and abiotic factors throughout their life cycle [5]. As such, a single genotype can produce multiple phenotypes

depending on the environment in which the plant grows (Figure 1.1). Plant phenotypes ultimately determine plant performance. Some examples of common plant phenotypes of interest include plant height, root diameter, root system architecture, strength, leaf color, cell size, grain yield, photosynthetic efficiency, chemical composition etc. Phenotyping (quantitative analysis and measurement of plant phenotypes) enables better understanding of plant structures and determination of their properties at different scales.

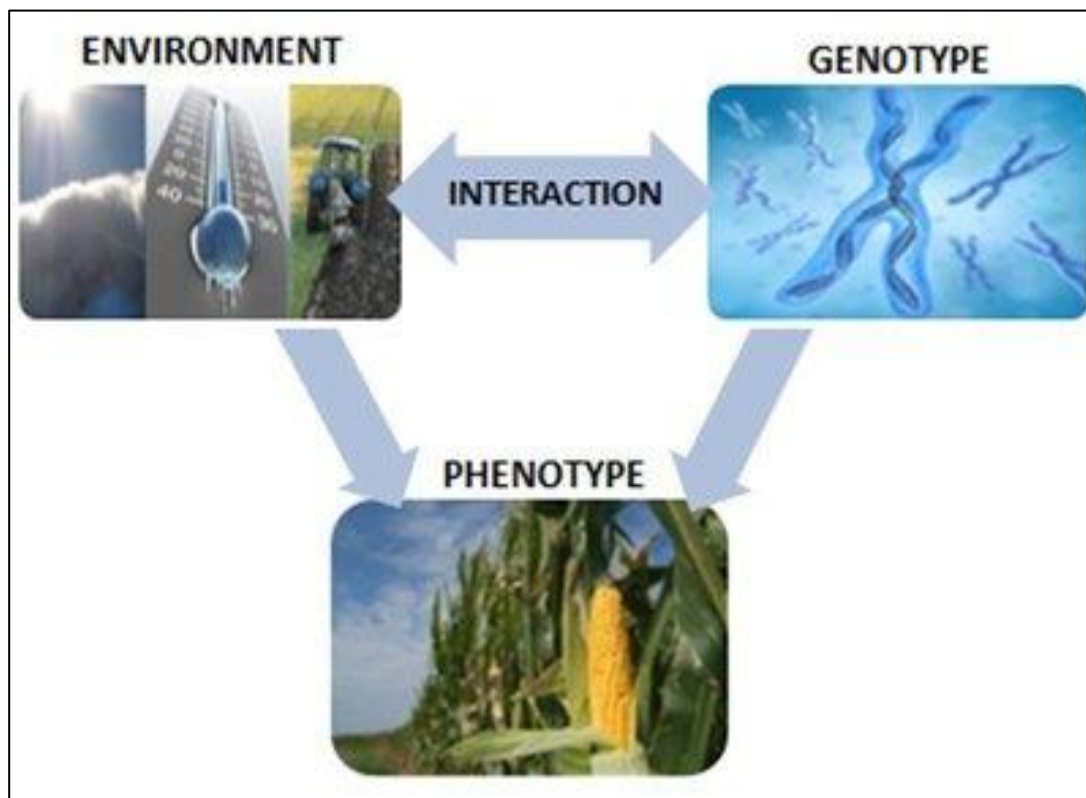


Figure 1.1: How Plant Phenotypes are Formed [6].

Plant phenotyping is an active area of research in the plant sciences. Plant phenotyping is the principle bottleneck preventing a greater understanding of plant science in general. Plant genotyping (sequencing DNA) has been automated in recent years and is now relatively inexpensive. In like manner measurements of weather and environment have largely been automated and are also relatively inexpensive and require minimal efforts in terms of human labor hours to collect. However, measuring physical characteristics of plants (phenotyping) is expensive, often requires manual labor and specialized equipment and expertise. Thus, phenotyping is the principle bottleneck preventing a

clearer understanding of how genotype and environment interact to determine plant performance (i.e., phenotype).

1.2 Crop Stalk Lodging

Wind damage has a major impact on numerous plants including crops and forests [15]. In particular, stalk lodging (mechanical failure of plant stalks during windstorms) is a multi-billion dollar a year problem experienced by many crops [7] (see Figure 1.2). Stalk lodging occurs when bending moments along the stalk induced by a combination of external forces (e.g., rain, wind) and body forces (e.g., plant weight) exceed the plant stalk's bending strength. This leads to stalk failure, typically in the form of buckling [1,7]. Several vital crop species that are key to maintaining global food and energy security are particularly prone to stalk lodging. For example, maize, rice, and wheat collectively account for two thirds, of human caloric intake [8] and are also used for biofuel production [9]. All three of these crops are severely affected by stalk lodging. Global annual yield losses due to stalk lodging ranges from 5 to 25% annually [10].

The study of plant biomechanics and in particular, development of cost-effective phenotyping strategies are key to addressing the problem of stalk lodging. The remainder of this thesis is focused on the development of a phenotyping methodology for efficiently quantifying plant phenotypes related to stalk bending strength (i.e., stalk lodging resistance). Five plant species were utilized as part of this thesis. These include, maize (*Zea mays*), sorghum (*Sorghum bicolor*), wheat (*Triticum aestivum*), poison hemlock (*Conium maculatum*), and Arabidopsis (*Arabis thaliana*). A brief description of the anatomy and major cell types of these plants is given below.



Figure 1.2: Stalk Lodging in Maize [11].

1.3 Plant Anatomy

A plant has four basic organs: roots, stalks, leaves, and flowers. These organs are in turn composed of tissues. Plant tissues are primarily composed of three different cell types. These are parenchyma, sclerenchyma, and collenchyma cells. A tissue could be simple (have one of these cell types) or complex (have two or more cell types). A brief description of each cell type is given below.

Parenchyma cells are found in parenchyma tissues and represent the majority (~90%) of the cells found in plants. They have thin primary cell walls and are mostly present in soft tissues. While their main function is nutrient storage, they also carry out majority of plant activities including photosynthesis. These cells are mainly found in stalks and roots.

Sclerenchyma cells are found in sclerenchyma tissues and represent about 10% of a plant. They have thick secondary cell walls. They provide mechanical strength and are primarily found in stems, roots, and leaves.

Collenchyma cells are the least common cell type representing only about 1% of cells in plants and are found in collenchyma tissues. They have uneven thickened primary cell walls and they mainly provide structural support in young stems and leaves.

Each of the plants included in this thesis have stalks that are composed of two or three major materials or tissue types, namely: rind, pith, and vascular bundles. Maize and sorghum have a pith while wheat, poison hemlock and Arabidopsis are hollow and do not possess a pith. The hollow plants (wheat, poison hemlock and Arabidopsis) have a dense outer rind sparsely populated with vascular bundles arranged in a ring-like manner [12] (see Figure 1.3). The rind makes up the outer shell of the stalk while the pith makes up the inner core of the plant. The rind is a tough, dense and stiff material that is composed mainly of sclerenchyma tissues and cells. It is the primary load bearing tissue in the stalk.

The tissue has a high stiffness. The rind provides mechanical support by bearing the compressive bending stress experienced by the stalk.

The pith is sparsely populated with scattered vascular bundles while the rind is densely populated with closely packed vascular bundles. The pith is a soft, foam like material, composed mainly of parenchyma tissues and cells. The mechanical function of the pith is to act as a mechanical brace to help increase stalk bending strength, prevent ovalization of the stalk cross section and buckling of the rind tissue.

Vascular bundles are composed of xylem and phloem tissues. These are complex tissues composed of cells with secondary cell walls. Xylem transports water from the soil to other parts of the plant while phloem transports the nutrients of photosynthesis from the leaves to other parts of the plants. These tissues help transport resources (water and nutrient) to the different parts of the plant and also provide structural support for the stalk.

All of the plant stalks investigated in this thesis can be separated into two distinct regions: nodes and internodes (see Figure 1.4). The nodes are small and very solid regions that act like mechanical bulkheads providing transverse bracing that resist buckling forces. Internodes are elongated prismatic regions that span between nodes.

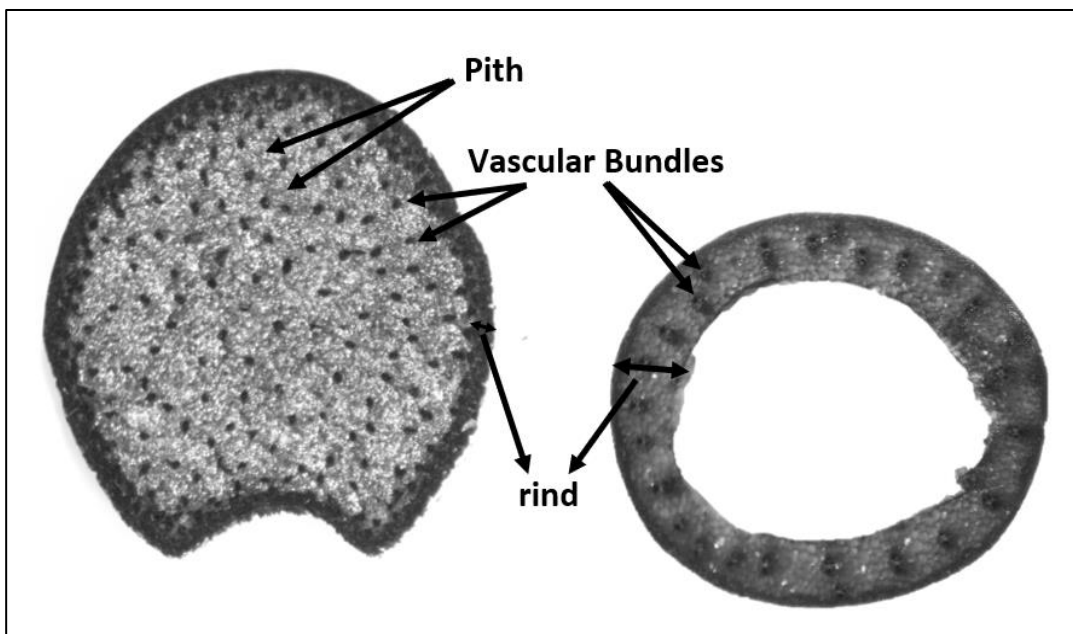


Figure 1.3: Safranin O and Alcian Blue Stained Cross-section of maize (left) and wheat (right) showing their tissue types.

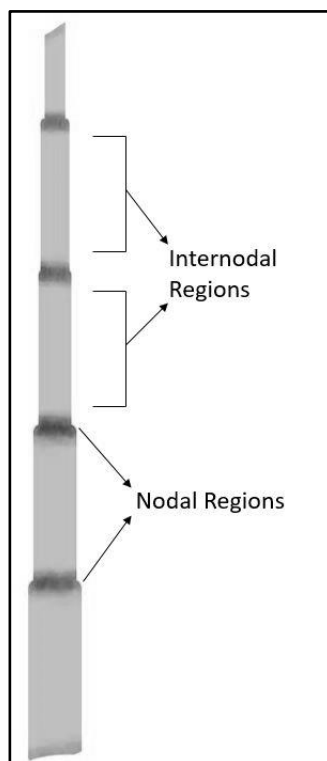


Figure 1.4: Typical profile of cereal crop stalks [13].

1.4 Problem Statement

As discussed in the previous sections, there is need for simple and cost-effective methodologies to quantify (i.e., to phenotype) the internal and external structures of plants in a high-throughput and cost-effective manner. This is needed not only to help address the problem of stalk lodging but also to advance our understanding in numerous areas of plant science and genome to phenome modeling. To this end, this thesis presents a phenotyping methodology for quantifying 2-dimensional plant cross-sections that offers reduced sample preparation time and does not require expensive imaging equipment. The method can quantify internal and external structures of plant cross-sections and enables researchers to easily import plant structures into third party software for further analysis. In particular, the algorithm can produce dimensionally accurate finite element models used to assess numerous biomechanical traits of plants. Chapter 2 presents a literature review of current methods of quantifying internal and external structures of plant cross-sections. Chapter 3-5 present the three parts of the newly developed methodology for quantifying cross-sectional structures in plants (sample preparation, image analysis and feature extraction). Chapter 6 demonstrates the exportation of plant structures into Abaqus for further analysis. Chapter 7 discusses future directions and recommendations.

Chapter 2: Literature Review

Several methodologies have been previously developed for quantitative phenotyping and analysis of internal and external plant structures (i.e., cross-sectional morphology). These methodologies can be generalized to consist of three distinct parts: 1) sample preparation, 2) image analysis and 3) feature extraction (see Figure 2.1). The following sections provide a brief review of each of these parts.

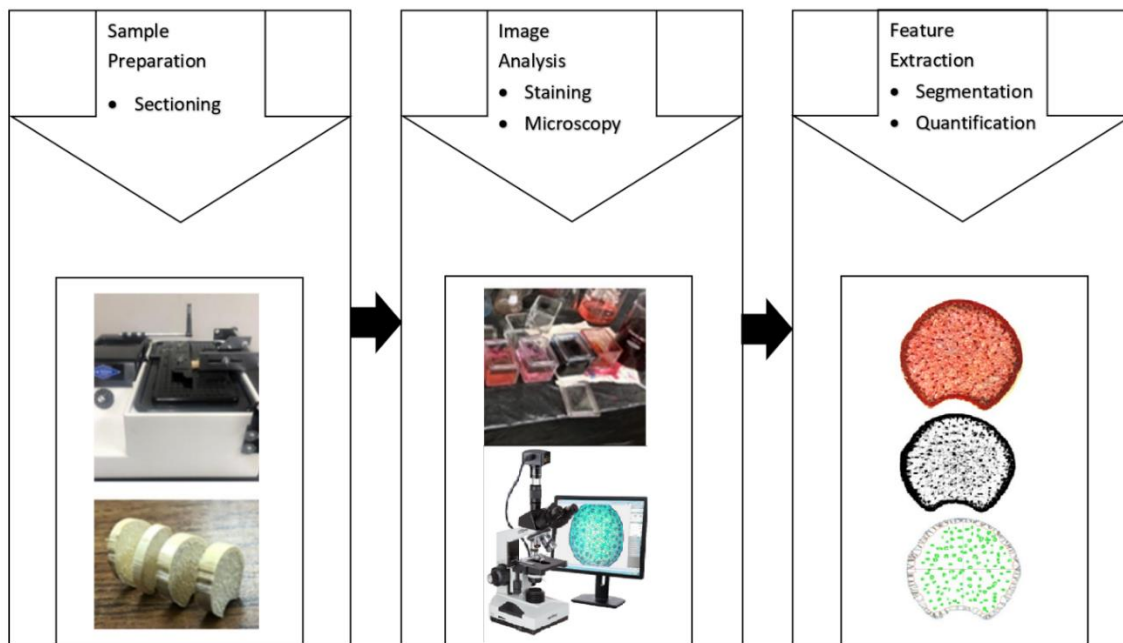


Figure 2.1: Workflow for Plant Phenotyping.

2.1 Sample Preparation

Plant samples must be properly prepared to ensure high quality images are obtained. Plant samples are prepared for imaging using several different techniques. These techniques are typically customized according to the particular imaging modalities that will be used. The techniques are designed to minimize any mechanical damage, modification, degradation, or contamination of the tissue samples of interest. The presence of vascular bundles in plants can make this especially challenging.

The majority of plant samples have vascular bundles which are present in the entire length of their stalks. These vascular bundles are composed of very hard and stiff tissue types which makes them extremely difficult to cut. This complicates sectioning of plant samples because these vascular

bundles are embedded in or surrounded by fragile plant tissues like the foam-like pith (see Figure 1.3). Attempts to cut these hard vascular bundles therefore results in deflections that induce damage in the surrounding softer tissues. These challenges have resulted in the development of time-consuming sample preparation protocols that preserve plant tissues and specialized equipment for cutting plant samples.

Most microscopy imaging modalities use histological sample preparation protocols. These protocols include fixing to preserve plant structures, dehydrating with alcohol to remove water from the specimen followed by clearing to remove residual alcohol from the specimen, embedding to hold specimens rigidly, sectioning to produce thin transparent sections and staining to highlight plant structures [14,15,16].

Plant sections prepared for light microscopy typically take hours to weeks to prepare depending on the specific embedding and sectioning steps employed. Most specimen sectioning is done using specialized tools like a vibratome or microtome – a machine used to cut thin slices (<50-100 μm) of material (see Figure 2.2). Non-embedded specimens cut with a vibratome take hours, non-embedded specimens cut with a microtome take days, and embedded specimens cut with a microtome take at least a week to prepare [19]. After undergoing these protocols, stained specimen sections are mounted for observation (i.e., imaging).

It should be mentioned that several imaging modalities exist that do not require extensive sample preparation work. In particular, freshly collected plant specimens can be imaged using Scanning Electron Microscopy (SEM), Transmission Electron Microscopy (TEM), Computed Tomography (CT) and Magnetic Resonance Imaging (MRI) [20,21,22]. These modalities require little to no sample preparation. However, they are not well suited to identifying many plant structures related to stalk bending strength [20,23]. Improved results can be obtained using computed tomography if specimens undergo fixation, dehydration and drying before imaging. These steps generally require at least three days to be completed [23].



Figure 2.2: A vibratome (Leica VT 1200S) [24] (left) and a microtome (Leica RM2245) [25] (right).

2.2 Imaging

Images of plant samples can be acquired using several different technologies. Technologies used determine the data sets of images produced. Scanning electron microscopy, computed tomography, and magnetic resonance imaging use beams of electrons, ionizing radiation, and radio frequency magnetic fields respectively to scan specimens and produce digitized three-dimensional volumetric data of plant specimens. Computed tomography and magnetic resonance imaging are categorized as non-invasive modalities (no physical sample sectioning required), allowing the entire sample to be imaged *in vivo*. 3D volumetric data obtained from these modalities are often virtually sectioned using applicable software [21].

Light Microscopy and transmission electron microscopy equipment transmit electrons and photons respectively through the specimen's surface to produce digitized two-dimensional cross-sectional images. These modalities require the plant sample to be cut into sections. In particular, $60\mu\text{m}$, $12\mu\text{m}$ and $1\mu\text{m}$ are generally recommended thickness for sections cut using a vibratome, microtome and ultra-microtome [19]. At these specimen thickness adequate imaging is achieved using light microscopy.

The imaging modalities mentioned above all offer different image resolutions and come with unique inherent costs. Electron microscopy produces the best resolution of 1nm . Light microscopy offers a resolution capacity of 200nm [22,23]. CT has a better image resolution than MRI at 300nm and $10\mu\text{m}$ respectively [23]. Figure 2.3, 2.4, and 2.5 show several commonly used imaging devices. These equipment are sophisticated and cost hundreds of thousands to millions of dollars [27,28,29,30]. However, light microscopy machines are not as expensive ranging between hundreds and thousands of dollars [31]. Significant costs are also associated with the sectioning. The thinner a

section needed, the more expensive the cutting equipment required. Hence, an ultra-microtome is the most expensive, while a microtome is generally more expensive than a vibratome. These pieces of cutting equipment cost tens of thousands of dollars [26].



Figure 2.3: A Scanning Electron Microscope (SEM) (JEOL JSM-7610F) showing its electron beam generator column, specimen chamber, vacuum pump, monitor, and control panels [32].



Figure 2.4: A Computed Tomography (CT) Scanner (GE Phoenix Nanotom System) showing its specimen cabinet [33].



Figure 2.5: A Magnetic Resonance Imaging (MRI) Scanner (Bruker Biospec Scanner) showing its specimen Chamber [34].

2.3 Feature Extraction

Procedures for image analysis and feature extraction can be classified according to the type of imaging sensor used or the data types being analyzed. Tools have been designed to extract phenotypic traits from both 2D and 3D datasets. Typical traits of interests include height, width, length, shape, area, and volume of various internal and external plant structures. Most image analysis software for plants are specialized to analyze specific plant parts of interest. For example, HTPPheno is commonly used for top and side view plant phenotyping of whole organisms. SmartGrain is frequently used to measure seed shape, while LAMINA is used to measure leaf shape [35,36,37]. The majority of image analysis tools for plants are dedicated to whole plant and external plant structure quantification. Relatively few are suitable for quantifying micro-scale or internal plant structures at the tissue or cell level [38]. Automated image processing workflows can be applied at the whole plant level using robotized platforms in growth chambers or greenhouses. However, automated imaging and analysis at the tissue level and cell level has yet to be achieved.

Image analysis processes generally involve segmentation, identification, extraction, and quantification of plant structures in acquired images. Images are commonly segmented using thresholding techniques. Plant structures are then identified by grouping thresholded areas of the image according to similar characteristics or abrupt changes in characteristics. Identified plant structures are classified and extracted by color, shape, edges, and textures [37]. Unwanted noise or details in and around extracted plant structures are cleared via filtering. Applicable measurements or quantification (e.g., counting) are carried out on extracted plant structures. These processes are developed to either operate in a manual, semi-automated or fully automated manner [38].

Major factors to consider in a plant phenotyping system include throughput, resolution, cost, and dimensionality [38]. Throughput being the amount of plants the system can analyze within a given period. Resolution refers to the system's capability to clearly depict plant structures at different scales. Dimensionality being the system's ability to measure diverse phenotypic traits. For example, several imaging technologies have been developed to offer high throughput using automated robotics and sensors [38,44]. However, this inherently limits their dimensionality. Thus, it is important to collectively consider throughput, resolution, and dimensionality.

These factors were considered in developing a method to phenotype internal and external structures of 2D plant cross sections. Phenotyping of plant cross section structures is typically accomplished via either: histologically prepared samples with microscopy imaging [45,46,47], hand

cut sections with flatbed scanner imaging [48] or Xray computed tomography imaging with virtual sectioning [21,49]. Histology and microscopy-based phenotyping typically requires at least a day for sample preparation and sectioning. Flatbed scanning is significantly faster and cheaper but has limited resolution and is not well suited to plants that are hollow or have smaller diameters. The Xray computed tomography methods requires expensive imaging equipment and typically requires hours to obtain an image depending on the desired resolution. To overcome some of the limitations associated with each of these modalities a new phenotyping method was developed. In particular, the new method presented in the following chapters is able to ensure quality image resolutions in a high throughput manner while significantly reducing sample preparation time and cost.

Chapter 3: Sample preparation

3.1 Samples

Dried plant stems were used as samples for this study. Plants analyzed included maize, sorghum, wheat, poison hemlock and Arabidopsis. The plants were classified into material type and size as shown in Table 3.1. Maize and sorghum plants consist of the rind, pith, and vascular bundles. Wheat, poison hemlock and Arabidopsis are hollow and do not contain a pith. Maize, sorghum, and poison hemlock have relatively bigger cross section in comparison to wheat and Arabidopsis. Figure 3.1 depicts the specific cross-sectional phenotypes of interest that were extracted from each plant sample.

Table 3.1: Plant Types and Descriptions

Plant Species	Number of Samples	Plant Parts/Materials	Phenotypes Quantified	Morphologies Extracted
Maize	8 varieties with 3 samples each	Rind, Pith and Vascular bundles	Major and minor diameter, Rind thickness, Number of vascular bundles	Rind boundaries, Vascular bundle boundaries
Sorghum	3 varieties with 2 samples each	Rind, Pith and Vascular Bundles	Major and minor diameter, Rind thickness, Number of vascular bundles	Rind boundaries, Vascular bundle boundaries
Wheat	1 variety with 10 samples	Rind and Vascular Bundles	Major and minor diameter, Rind thickness	Rind boundaries
Poison Hemlock	1 variety with 10 samples	Rind and Vascular Bundles	Major and minor diameter, Rind thickness	Rind boundaries
Arabidopsis	1 variety with 10 samples	Rind and Vascular Bundles	Major and minor diameter, Rind thickness	Rind boundaries

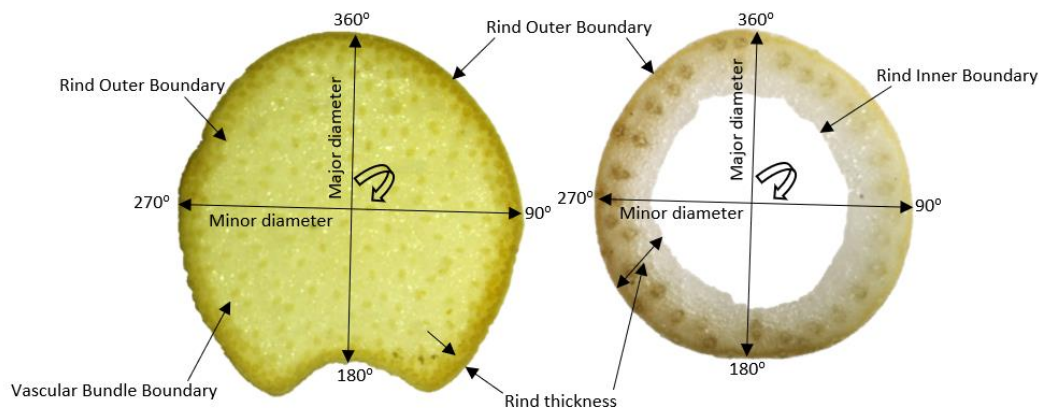


Figure 3.1: Phenotypes Extracted and Measurements Taken for Maize (left), and wheat (right).

3.2 Sample Sectioning

Multiple methods of sectioning plant samples were investigated. The aim was to develop a quick, efficient, and inexpensive cutting method. Sectioning methods were evaluated based on the quality of the plant section produced and the time required to produce the section. Common problems encountered when trying to section plants included pulled vascular bundles, frayed or ripped rind material and vascular bundles, burnt imaging surface, uneven imaging surface, and crushed cross-sections. These problems were mostly due to the hard and stiff vascular bundle tissues deflecting or getting pulled during cutting operations thereby inducing damage in the soft and fragile tissues they are surrounded by.

Several cutting tools were investigated and are shown in Figure 3.2. the first cutting tool investigated was a chop saw (Makita 2414DB Cut-Off Saw) with a 14" abrasive cut-off wheel, which rotated at 3800rpm. The chop saw's built-in vise was used to hold the samples in place while cutting. The second cutting tool investigated was an angle grinder (Metabo WEV15-125 Angle Grinder) with variable speed and a 5" blade diameter. The angle grinder was mounted on a pivoted angle grinder stand to enable easier cutting of clamped samples as shown in Figure 3.2. Three blade types and various cutting speeds were investigated with this machine. The third cutting tool investigated was a water jet cutter (Omax Model 55100). Plant sections were produced with the waterjet on the fiberglass cutting setting. The fourth cutting tool investigated was a trim saw (Hi-Tech Diamond 6" Trim Saw). It was set up as shown in Figure 3.2, with a Hi-tech Diamond Silver Thin Notched Saw Blade, which rotated between 800-4000rpm, a saw fence (Hi-Tech Diamond 70-300) and a saw vise

(Hi-Tech Diamond 22-331). Lastly the ability of a simple razor blade (Van Der Hagen Stainless Razor Blades) to cut plant sections was investigated.

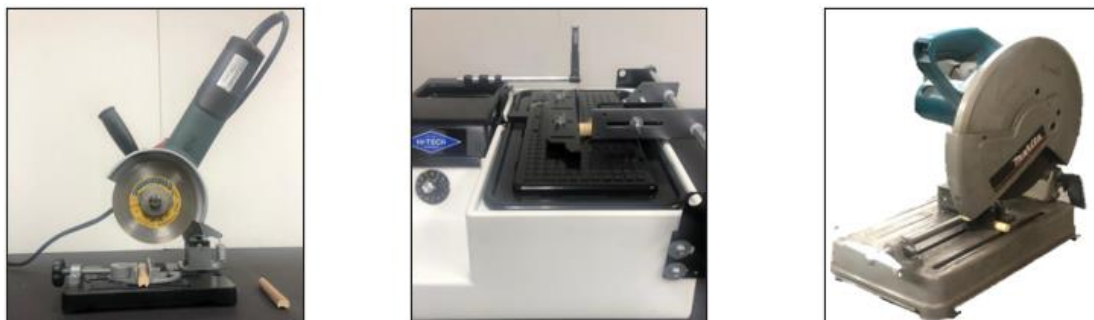


Figure 3.2: Machine set-ups for sectioning samples. Set-up of Metabo WEV15-125 Angle Grinder (left), Set-up of Hi-Tech Diamond 6" Trim Saw (center) and Set-up of Makita 2414DB Cut-Off Saw (right).

3.3 Sample Sectioning Results

All the power cutting machines except the trim saw encountered several problems while trying to section the plants. As seen in Table 3.2 and Figure 3.3, the chop saw, angle grinder and water jet machines produced unacceptable sections. The angle grinder was operated at about 3000rpm with three different blades. A tile blade produced best results with the angle grinder as it prevented burning the surfaces and ripping the rinds of sections. However, the tile blade pulled the vascular bundles embedded in the pith and this subsequently led to blurry images. Using the chop saw and the angle grinder with a coarse blade did not prevent any of the sectioning issues. While water jet cutter required relatively long time periods to produce plant sections, it produced unburnt and undamaged plant sections. However, the surfaces of plant sections produced with the water jet cutter were uneven (see Figure 3.3) which caused reduction of image quality. The trim saw was the only machine that was able to produce acceptable plant sections for imaging maize, wheat and poison hemlock.

Table 3.2: Evaluation of Cutting Machines for Plant Sectioning

Problems	Causes	Chop Saw	Angle Grinder			Trim Saw	Water Jet
			Coarse Blade	Fine Blade	Tile Blade		
Burnt section surface	Blade surface	x	x				
Ripped rind	Blade type/speed	x	x	x			
Pulled vascular bundles	Blade type/speed	x	x	x	x		
Blurry images	oblique sections	x	x	x	x		x

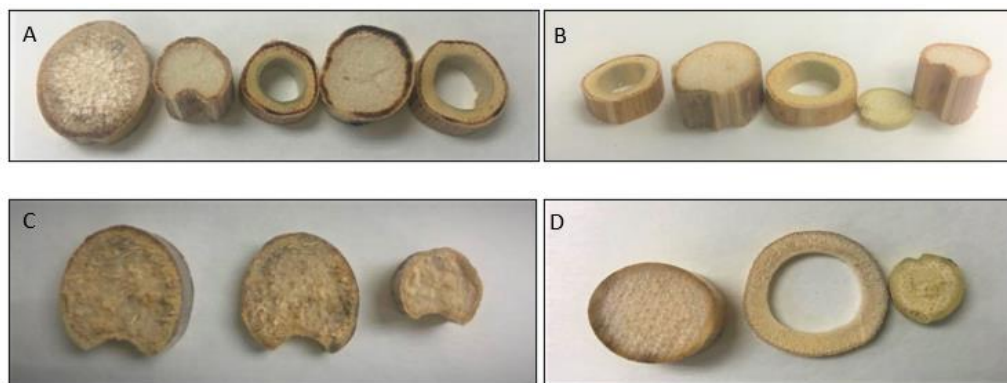


Figure 3.3: Problems encountered while sectioning; A) Burnt/stained section surfaces, B) sections with ripped rinds, C) Sections with pulled vascular bundles D) oblique section surfaces.

None of the above machines (including the trim saw) were able to provide quality sections of wheat and Arabidopsis plant stems. These plants are relatively small, have a softer rind and possess a hollow fragile structure. Thus, a different sectioning approach was required for these plants than was required for maize, sorghum, and poison hemlock. In particular, sections of wheat and Arabidopsis

plant stems were cut using a razor blade (Van Der Hagen Stainless Razor Blades). However, the wheat and Arabidopsis samples had to be hydrated before being sectioned. This reduced friction and enabled easier cutting of thin sections. After hydrating the plant by immersing it in distilled water. The plant was held firmly with the thumb and index fingers in one hand and cut with the other. The blade was held perpendicular to the sample. Multiple sections were created simultaneously by drawing the razor blade through the sample. For wheat plants, to prevent the effects of shadows during image processing, plant sections had to be between 1mm and 2mm thick. It was important to avoid any sawing motions while cutting sections and instead chop down in one single smooth motion. This prevented ripped rind and sample damage. Cutting of oblique sections was avoided by ensuring the razor was not bent while cutting. The razor blades had to be replaced after cutting an average of ten plant sections. It should be noted that the razor blade was unable to provide suitable sections for maize, poison hemlock or sorghum. When attempting to cut these plants with a razor blade, the plants would simply crush and the blade was ineffective in cutting through the tough vascular bundle and rind tissues. Specific sectioning protocols used for the plant species in this thesis can be found in Appendices A, B and C.

3.4 Recommended Practices for Sectioning

Testing revealed the optimal blade type for sectioning was smooth, toothless, and unpainted. The cutting machine should have an adjustable speed to prevent burning the plant sample and the capability to cut straight parallel sections. The trim saw meets these criteria and produced the best sections of maize, poison hemlock and sorghum. Plant samples were cut at speeds of approximately 800-1000rpm depending on the hardness of the plant stalk's rind. The saw fence (Hi-Tech Diamond 70-300) and saw vise (Hi-Tech Diamond 22-331) ensured the cutting of parallel and thin 2-4mm sections. This cutting method requires little training and enables quick sectioning of plant stalks in minutes which was a significant reduction from the typical one-week period required by most histological sample preparation protocols. A razor blade was the best tool for cutting quality sections of the wheat and Arabidopsis plants. To produce parallel sections with even imaging surfaces, it was essential to ensure repeatedly cutting adjacent sections by chopping down in a single smooth motion without any back-and-forth sawing motion.

Chapter 4: Image Analysis

4.1 Specimen Staining

Sectioned specimens are frequently stained to improve contrast between plant structures thereby enhancing image analysis and feature extraction. The ability of Safranin O, Alcian Blue and Toluidine Blue stains to increase contrast between plant structures were investigated as part of this thesis. These are some of the most prominent stains used for studying the anatomy of biological tissues [15]. Safranin O and Alcian Blue have affinity for lignin and cellulose respectively [15]. Safranin O solution stains plant structures red whereas Alcian Blue stains plant structures blue. Toluidine Blue can stain plant structures green, blue, purple, red or pink depending on their reaction with Toluidine Blue. . Alcian Blue solution was made by mixing 3grams of Alcian Blue, 250ml of distilled water, 6 drops of glacial acetic acid and 4ml of formaldehyde 40% solution [50]. Safranin O Solution was made by mixing 3grams of Safranin O, 100ml of Methylated Spirit, 100ml of distilled water and 2ml of formaldehyde 40% solution[50]. Toluidine Blue solution was made by dissolving 1gram of toluidine blue in 100ml of distilled water [51].

Both simple and differential staining techniques were investigated to determine a staining sequence that would produce the highest contrast between plant structures of interest. Differential staining applies multiple sequential stains to the plant section (i.e., staining and counter staining) whereas simple staining procedures employ only one stain. For differential staining, stains were chosen according to their compatibility and their high affinity to selectively stain different plant structures. The staining protocol for all specimens included hydrating specimens in distilled water, staining specimens by submersion in a solution, rinsing in distilled water to remove excess staining solution followed by dehydrating the specimen in alcohol. Specific staining protocols used for the plant species in this thesis can be found in Appendices A, B and C. The time required to complete each step was investigated and was varied to reveal the sequence that would provide optimal contrast between plant structures in minimal time.

4.2 Recommended Practices for Specimen Staining

After undergoing the simple staining technique, both rind and pith materials in maize and sorghum were stained in the same color. The rind and vascular bundles were generally stained darker than the pith (e.g., see Figure 4.1) thereby increasing contrast. However, in stained sorghum sections a clear delineation of the boundary between the pith and the rind was not obtained and

vascular bundles were also not adequately stained in Arabidopsis sections. When staining wheat and poison hemlock sections, plant structures appeared in similar colors while the vascular bundles appeared in darker shades of the same color as can be seen in Figure 4.2.

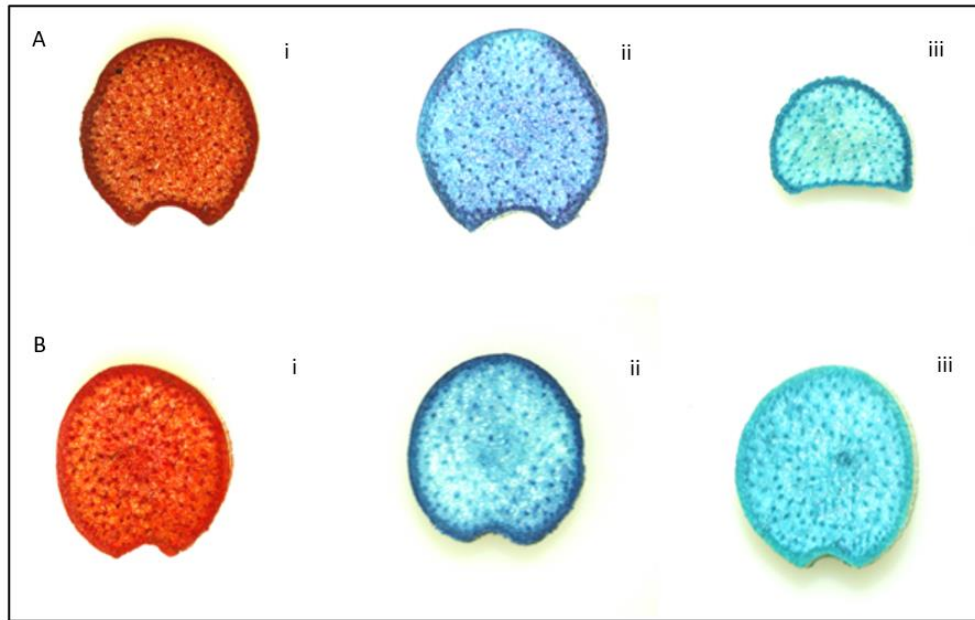


Figure 4.1: Plant sections of A) Maize and B) Sorghum stained with i) Safranin O, ii) Toluidine Blue and iii) Alcian Blue.

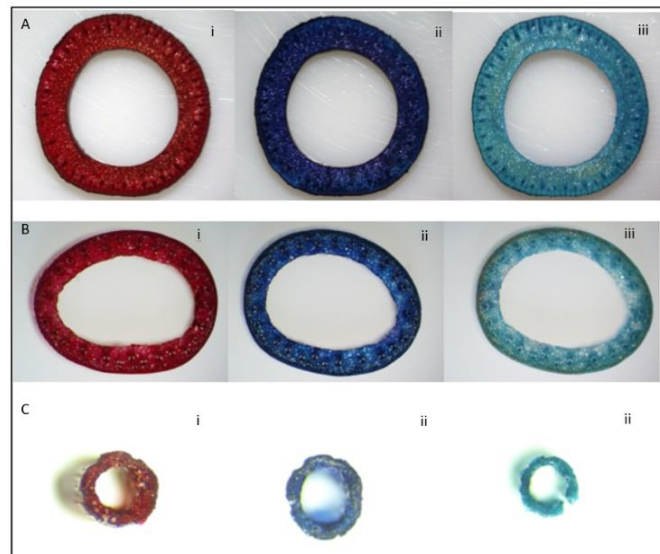


Figure 4.2: Plant sections of A) Poison Hemlock, B) Wheat, C) Arabidopsis stained with i) Safranin O, ii) Toluidine Blue and iii) Alcian Blue.

Differential staining techniques were applied to sectioned specimens using Alcian Blue and Safranin O stains. Staining of specimens was achieved by following the Alcian Blue-Safranin O staining sequence (Figure 4.3) presented in [50]. As seen in Figure 4.4, investigations revealed that the differential staining technique was more effective, it produced specimens with a clear delineation of the boundary between the pith and rind for pith filled plant specimens and increased contrast between plant structures of single material plant specimens.

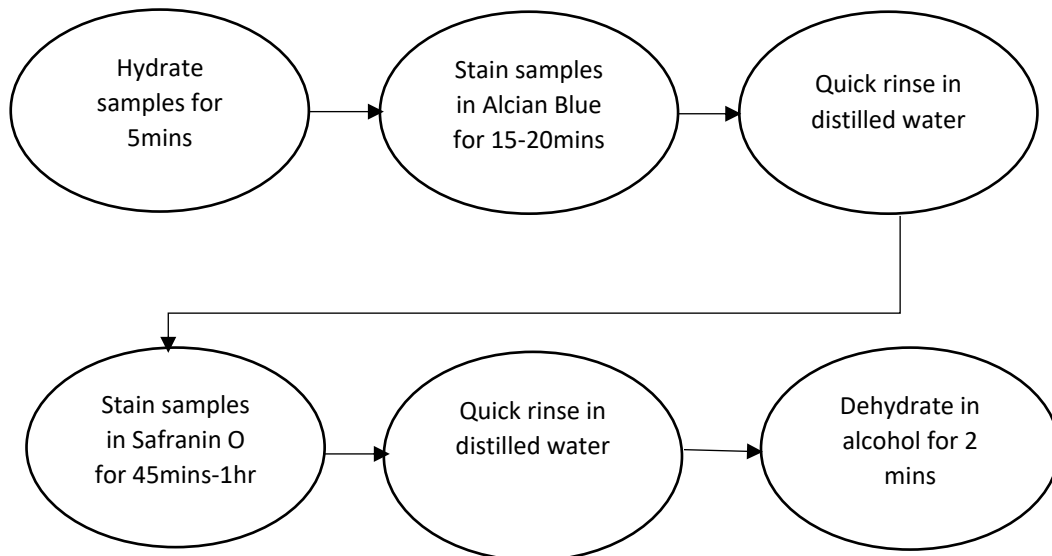


Figure 4.3: Alcian Blue-Safranin O Staining Sequence

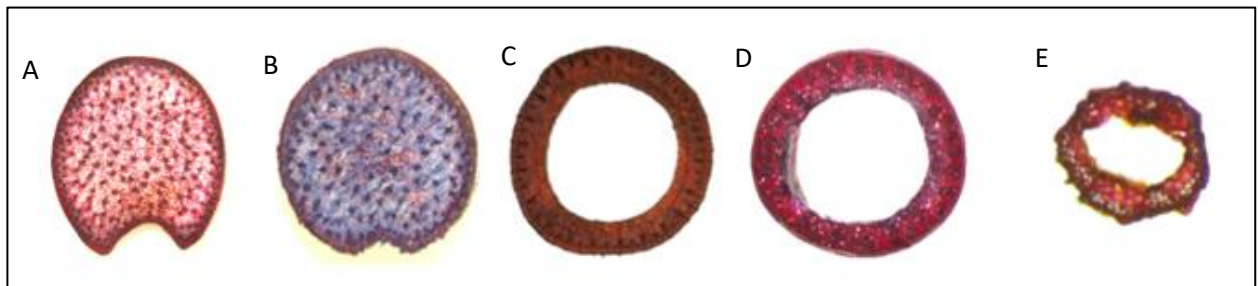


Figure 4.4: A) Maize, B) Sorghum, C) Poison Hemlock, D) Wheat and E) Arabidopsis samples stained using the Safranin O-Alcian Blue Staining Sequence.

4.3 Imaging

Imaging involved the digitization of stained sectioned specimens. The aim was to provide an inexpensive and simple method to acquire quality images. A decision-making process was implemented to select the most suitable microscope for this application. Factors considered included: wide field of view to capture the whole cross section of large, sectioned specimens, quality image resolution to enable easier image processing, camera software interface to enable better user experience and flexible magnification to enable imaging of different sized plants.

4.4 Recommended Practices for Imaging

Images acquired using a flatbed scanner did not produce the required contrast for effective image processing. As seen in Figure 4.5, it was difficult to segment the rind from pith because the rind color blends with the background of images captured. The scanner was also incapable of capturing Arabidopsis and wheat sections at required resolution due to their small sizes.

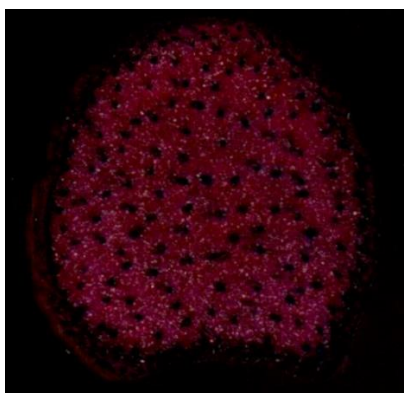


Figure 4.5: Image of stained section obtained using a flatbed scanner (hp LaserJet)

After consideration of the factors mentioned above to ensure effective microscopy imaging. A stereo microscope was selected as the best imaging option. The microscope accessories had several accessories that simplified imaging and enabled inspection of thicker specimen sections. The microscope was an AmScope LED Trinocular Zoom Stereo Microscope as shown in Figure 4.6, along with its 0.5X and 2.0X Barlow lenses and an 18MP digital camera. The first step of the imaging process was to ensure the sharpest (i.e., focused) image of the stained specimen was viewed on the AmScope camera software interface (Toupview) before capture. The next step was to calibrate the microscope to ensure accurate conversion of specimen sizes. This was done using a scale rule to obtain the number of pixels equal to 1mm. After calibration, specimen images were captured using

the digital camera in combination with the AmScope software interface. Each image was saved in tagged image file (tif) format with a dimension of 4912x3684 pixels and resolution of 96dpi. Specific imaging protocols used for the plant species in this thesis can be found in Appendices A, B and C. The microscope had an objective lens with 0.7 to 4.5 magnification power when used along with its 0.5X and 2.0X Barlow lenses. The 0.5X lens enabled a large working distance for easy adjustment of specimens and a wider field of view for the large cross section of maize, sorghum, and poison hemlock specimens. The 2X lens enabled extra zoom to capture smaller sized wheat and Arabidopsis samples. Images obtained were sharp and provided clear contrast which simplified image processing.



Figure 4.6: 3.5X-180X Trinocular Stereo Microscope with 18 MP Camera (left) and Barlow lenses 0.5X (middle) for wide field of view and 2X (right) for better magnification.

4.5 Recommended Practices for Image Analysis

The differential staining technique produced required contrast between plant structures of both single and composite plant specimens whereas the simple staining techniques was relatively ineffective. The Alcian Blue-Safranin O sequence was selected as the best universal staining method for all plant species included in this thesis as it ensured clear delineation of the boundary between the rind and pith tissues as well as identification of vascular bundles within the pith and the rind as shown in Figure 4.4. The stereo microscope was inexpensive and required little training to operate. It produced sharp quality images that enabled identification of plant structures in stained sections. The microscope's camera software calibration process was simple and quick and enabled automatic batch saving of captured images.

Chapter 5: Feature Extraction

Feature extraction from digitized plant images consists of four parts, namely: pre-processing, segmentation, smoothing, and quantification. The MATLAB (MATLAB R2019a) computer programming software was used to develop an algorithm to implement each of these steps. The MATLAB code can be found in Appendices D and E. The MATLAB feature extraction algorithm was customized according to the single and composite material plant types. Specific image processing protocols used for the plant species in this thesis can be found in Appendices A, B and C.

5.1.1 Pre-processing

Pre-processing consisted of separating the pixels of digital images into groups to aid in distinguishing between different plant structures. To accomplish this the captured Red, Green and Blue (RGB) digital image was first converted to a grayscale image. This conversion reduced the red, green, and blue intensity channels to one intensity level per pixel. Pixels were then grouped according to their pixel intensity values using local adaptive thresholding [52] and otsu thresholding [53] for composite and single material plant types respectively. Optimum threshold values were automatically calculated and applied to different regions of the image to aid in identifying plant structures. The image was then binarized to consist of either black or white pixels.

5.1.2 Segmentation

Segmentation involved identifying and separating different plant structures from the binary image. Maize and sorghum binarized sections were segmented into two different areas. The largest area (whole cross-section) in the binary image and the second largest area (the pith). Single material plant types were segmented into their hollow and whole cross-sectional areas. To ensure adequate identification and measurement of plant structures, image smoothing was applied to segmented areas.

5.1.3 Smoothing Operations

Smoothing operations were implemented to remove unwanted details from segmented images. Unwanted details were identified as objects in images with very small area. They were either holes (white pixel objects) or noise (black pixel objects). The fill and erosion operations were used to fill up holes and remove noise respectively [54]. Both processes required creating a new structuring element – an object with a specified radius or area, which is placed at the center of each object in the

image to be smoothed [54]. Any image object smaller than the newly created object automatically picks up the pixel of the newly created object.

5.1.4 Quantification

Quantification involved the extraction and measurement of identified plant structures. The rind boundary coordinates of both composite and single material plant types were used to quantify stalk diameters and rind thickness. The major and minor diameter endpoints were calculated using the rind outer boundary coordinates at 90°, 180°, 270° and 360° as shown in Figure 3.1. The rind thickness was calculated as the mean of the shortest distance between each pair of the inner and outer boundary coordinates. These diameter and rind thickness measurements were validated in comparison to digital calipers measurements. The major and minor diameter were measured with digital calipers using the same points and orientation of the acquired image read into the image processing algorithm. The average rind thickness of each specimen was calculated by taking digital caliper measurements of the rind thickness at 90°, 180°, 270° and 360° as shown in Figure 3.1.

In maize and sorghum sections, vascular bundles were quantified using a semi-automatic approach. First, the number of vascular bundles was automatically quantified. Then closely packed collectively identified vascular bundles were deleted and individually re-selected. At this time any omitted bundles were also selected. The boundary of each vascular bundle was also extracted. These extracted rind and vascular bundle boundaries were imported into third party software for further analysis.

5.2 Feature Extraction Results

During the pre-processing step, the raw red, green, and blue digital image was converted to a binarized image as shown in Figure 5.1. The binary images of the plant sections were subsequently segmented (Figure 5.2). The whole cross-sectional area and pith area of binarized sorghum and maize sections were segmented into two different images. Wheat, Arabidopsis, and poison hemlock binarized images were segmented into their whole and hollow cross-sectional area. This step generally revealed hidden unwanted elements in the whole cross-sectional areas.

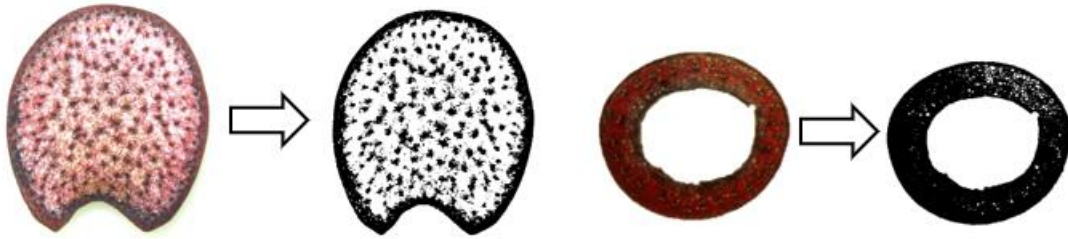


Figure 5.1: Raw (RGB) image and thresholded (binarized) image of maize (left) and wheat (right) sections

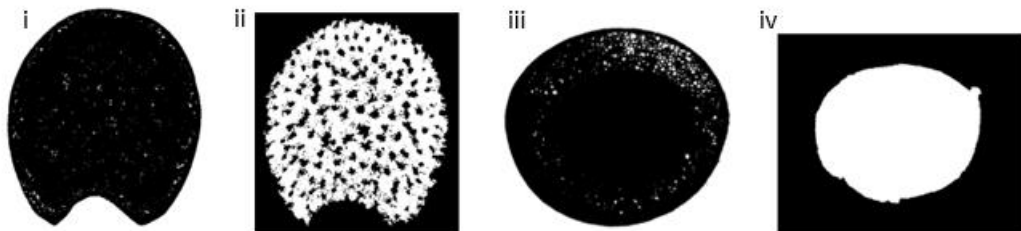


Figure 5.2: Segmented areas: i) maize whole cross-sectional area ii) maize pith area iii) wheat whole cross-sectional area iv) wheat hollow area.

After applying the preprocessing and segmentation steps of the feature extraction algorithm the rind and vascular bundles of the plants were composed of black pixels while the pith and hollow center of the plants were composed of white pixels (see Figure 5.2). However, the binarized images of both plant types possessed unwanted elements (small white elements in the rind and small black elements in the pith). The noises and holes in the rind and pith segmented areas as seen in Figure 5.2 (i), (ii) and (iii) were cleared during smoothing operations. Figure 5.3 shows smoothed images after fill operations were applied. This subsequently enabled adequate extraction of rind boundaries followed by quantification of applicable phenotypes.

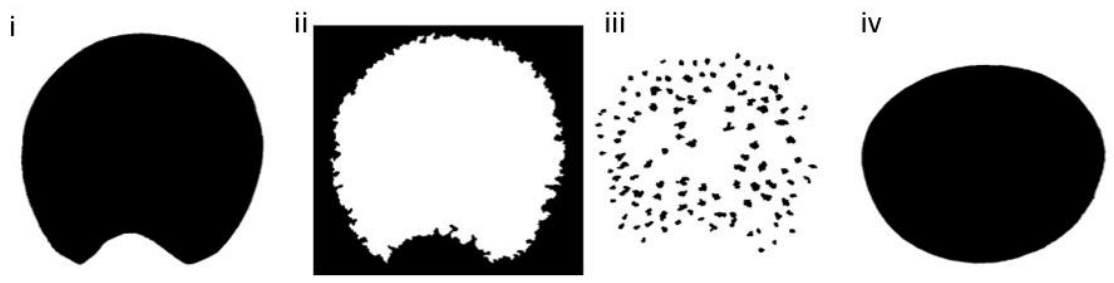


Figure 5.3: Smoothed images of i) maize whole cross-sectional area, ii) maize pith area, iii) vascular bundles within maize pith and iv) wheat whole cross-sectional area.

Figure 5.4 shows the major and minor diameter lines as well as the rind and vascular bundle boundaries. The average length of the lines plotted between rind boundaries as shown in Figure 5.4 was calculated as the rind thickness of plant sections. Automatically identified and manually selected vascular bundles and their boundaries are shown in Figure 5.5. The vascular bundle boundaries were overlaid on the section's grayscale image to enable easier manual verification and selection. Circles were plotted around the selected vascular bundles as shown in Figure 5.5.

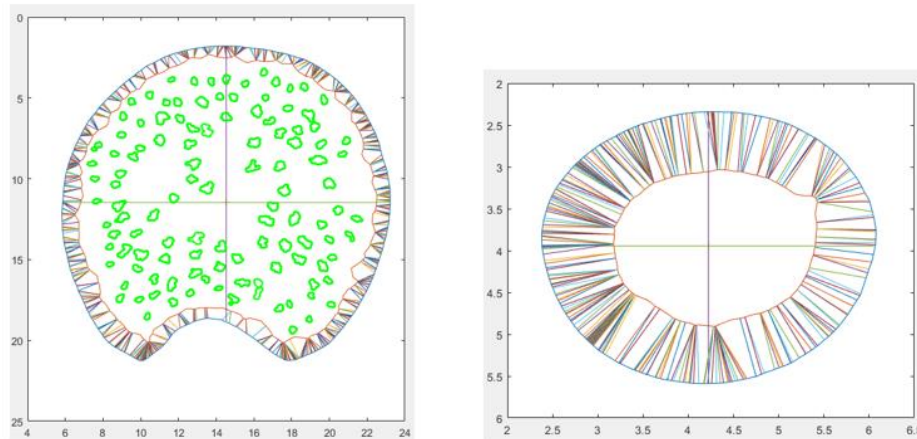


Figure 5.4: Maize section (left) and wheat section (right) showing extracted rind boundaries, major and minor diameter lines, rind thickness measurement lines and maize vascular bundle boundaries (left).

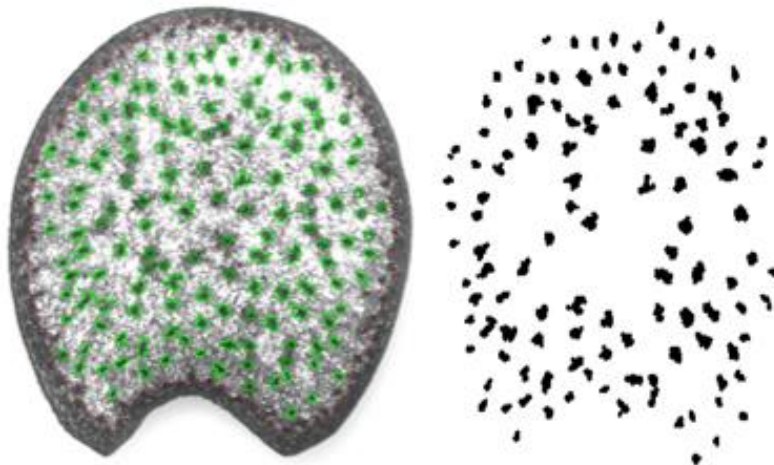


Figure 5.5: A maize section's automatically identified vascular bundles (right) and its grayscale image with overlaid identified vascular bundle boundaries and plotted circles for manually selected vascular bundles (left).

Each phenotype obtained by the newly developed image analysis algorithm was compared to traditional manual measurements. As can be seen in Figures 5.6 – 5.9 results from the image analysis algorithm were in good agreement with manual measurements. In particular, linear correlations analysis demonstrated R^2 values of 0.9697, 0.9712, 0.9494 and 0.9235 for the major diameter, minor diameter, rind thickness and vascular bundle count, respectively.

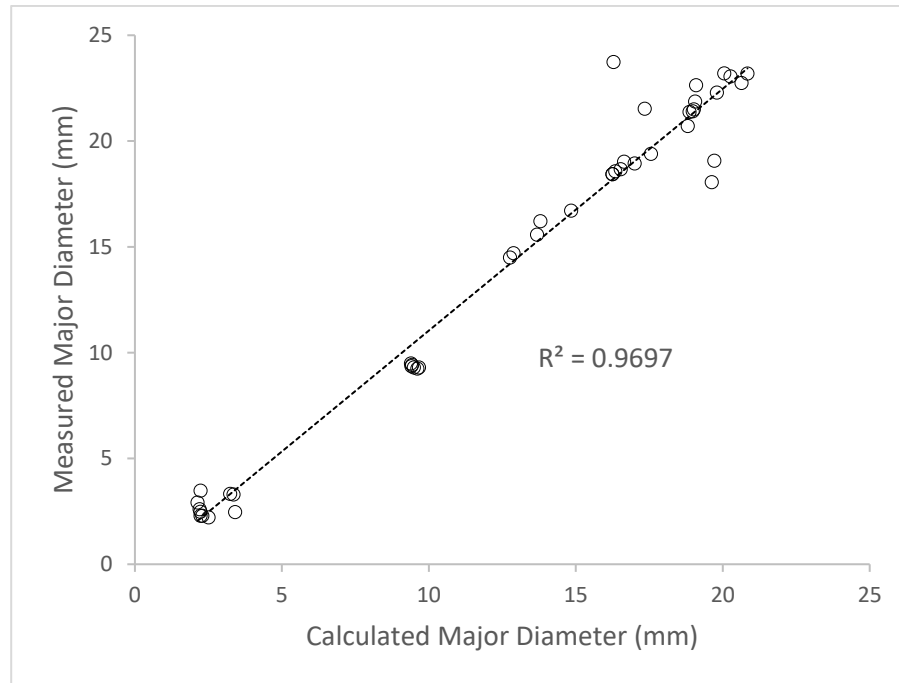


Figure 5.6: Measured vs calculated major diameter measurements of wheat, sorghum, maize, and poison hemlock.

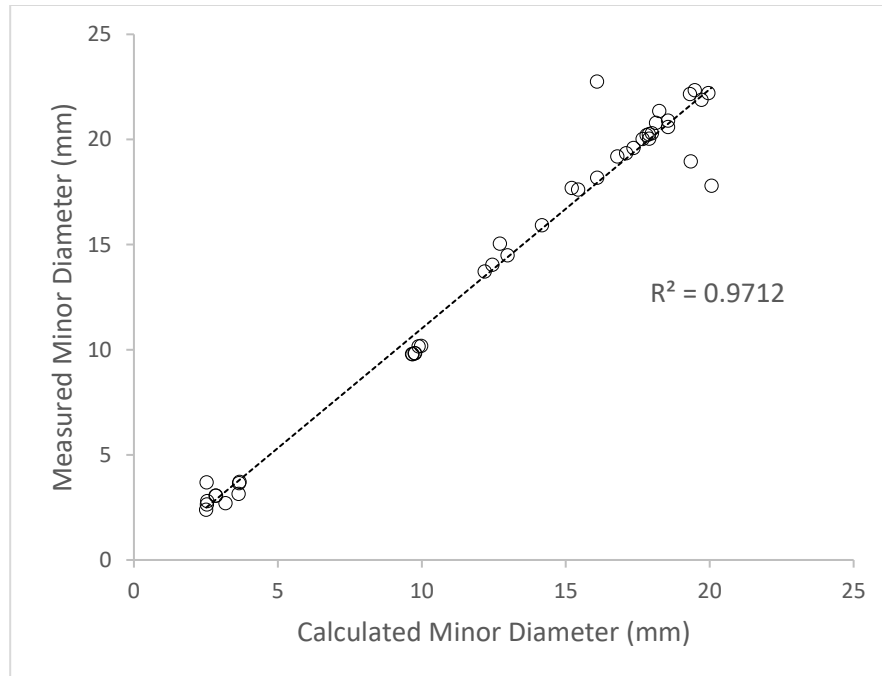


Figure 5.7: Measured vs calculated minor diameter measurements of wheat, sorghum, maize, and poison hemlock.

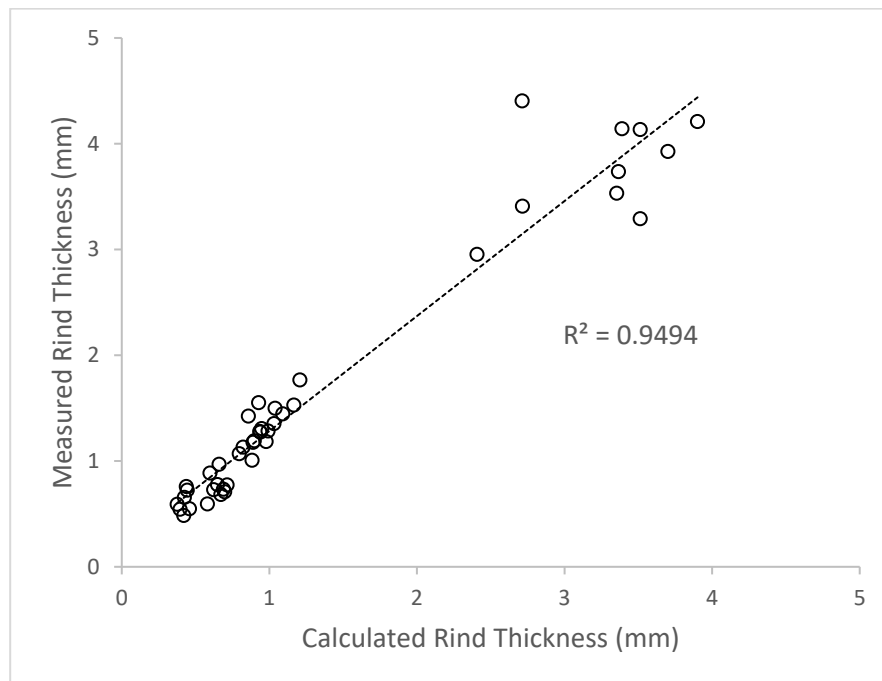


Figure 5.8: Measured vs calculated rind thickness measurement of wheat, sorghum, maize, and poison hemlock.

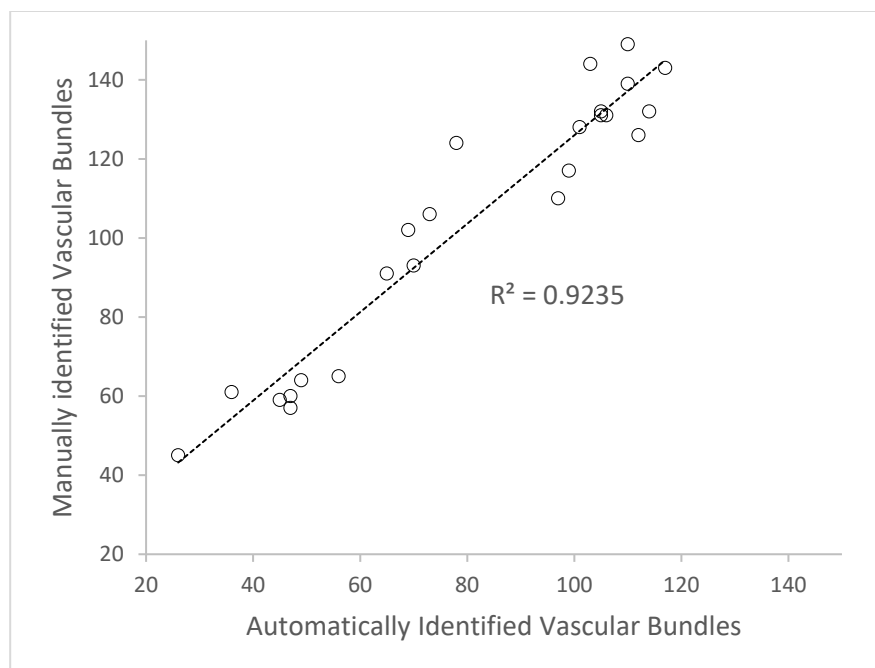


Figure 5.9: Manually Identified vs Automatically identified vascular bundles from maize and sorghum piths.

5.3 Comparisons Among Plant Samples

The aim of this thesis was to develop a fast, simple, and inexpensive phenotyping methodology to quantify the internal and external structures of plant stalks. This methodology was applied to 8 varieties of maize, 3 varieties of sorghum, 1 variety of wheat, 1 variety of poison hemlock and 1 variety of Arabidopsis stalks.

The obtained phenotypes for maize and sorghum include major and minor stalk diameter, number of vascular bundles and rind thickness as shown in Figure 5.10 and Figure 5.11. For wheat, poison hemlock and Arabidopsis the rind thickness, minor and major diameter were obtained. The three varieties of sorghum were Ram, Simon, and Smith stalks. Results showed that Ram stalks had the largest cross-sectional area, followed by Simon and Smith stalks, respectively. Simon stalks had the highest number of vascular bundle count with 53 vascular bundles on average, Ram had 36 and Smith had 42. Smith stalks had the thinnest rind at 0.63mm, Ram stalks had 0.69mm rind thickness and Simon stalks had 0.64mm rind thickness. The eight maize varieties sampled were B73 NOPOL, B73 POL, B73xMo17 NOPOL, B73xMo17 POL, Mo17xB73 NOPOL, Mo20W POL, Mo17 NOPOL and Mo17xB73 POL. Mo17 NOPOL had the least number of vascular bundles with 80 and B73xMo17 NOPOL had the most with 134. Mo17xB73 NOPOL had the largest cross-sectional area with 131

vascular bundles while B73 POL had the least cross-sectional area with 102 vascular bundles. Mo20W POL had a rind thickness of 1.21mm which was the thickest and B73xMo17 NOPOL had the thinnest rind at 0.84mm.

The average major and minor diameter of poison hemlock stalks were 18.54mm and 18.13mm respectively and their average rind thickness was 3.26mm. The wheat variety had average major and minor diameter of 2.59mm and 3mm respectively and average rind thickness of 0.5mm. Arabidopsis samples had an average rind thickness of 39.62 microns and major and minor diameter of 286.33 microns and 218.14 microns, respectively.

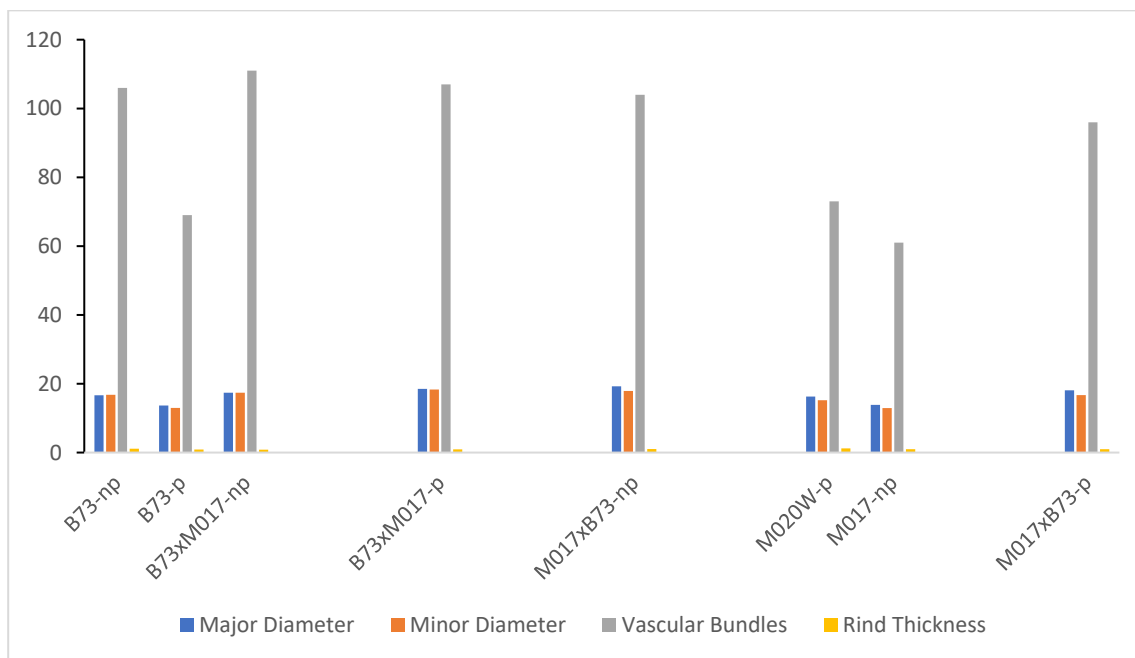


Figure 5.10: Quantification of phenotypes obtained for maize varieties using image analysis algorithm

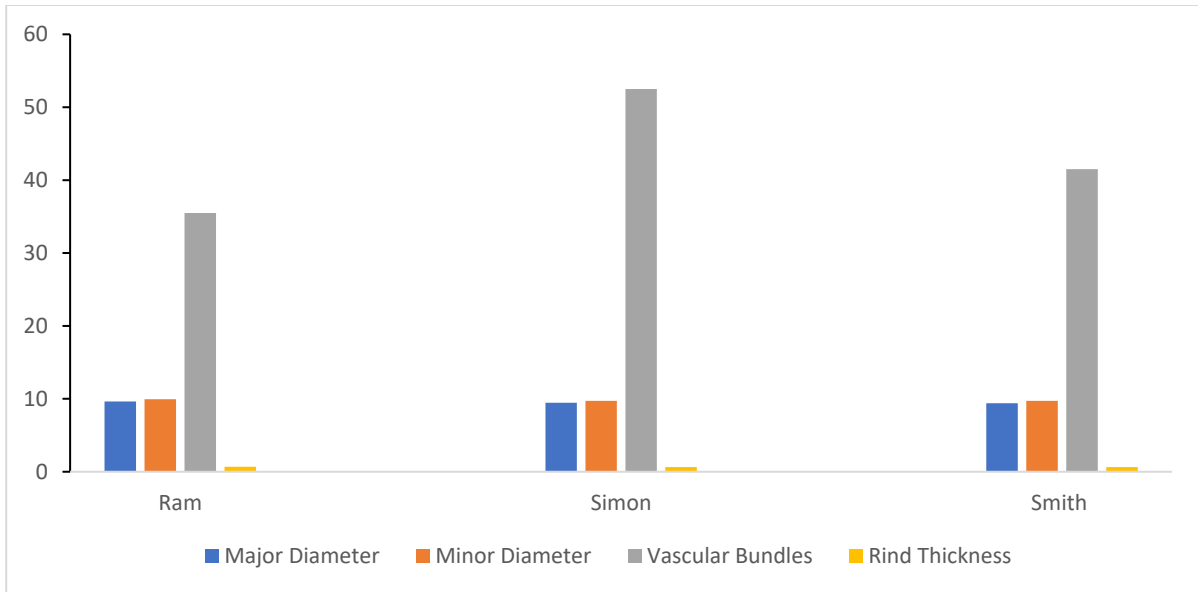


Figure 5.11: Quantification of phenotypes obtained for sorghum varieties using image analysis algorithm

Chapter 6: Exporting Extracted Plant Features to Third Party Software

Finite element analysis (FEA) can be implemented to assess biomechanical traits of plant structures and improve plant performance. FEA models of plants are developed to enable better understanding of the stress, strain, force, and displacement experienced by plants. In particular, structural analyses of plant stems have been performed using computational models to analyze the failure modes or mechanisms of stems [56,57,58]. Plant stems are known to fail mainly due to the bending stresses they experience, and the major failure mode is transverse buckling which is due to the stem's cross section ovalizing [59,60]. Consequently, accurate model geometry is very important when performing structural analysis of plant stems. Geometry definition is the first primary step in developing computational models. Plant stems are often modeled using circular cross sections or specimen specific geometry extracted from plant specimens scanned using computed tomography [57,59]. The later requires very expensive equipment and specialized expertise as discussed earlier while the former entails assumptions which might not produce accurate results. The methodology developed for this thesis enabled the extraction of cross-sectional geometries from plant specimens. These geometries were imported into finite element software to analyze the different plant stems. The scripts developed for importing the plant geometries and examples of the resulting finite element models are described in the following sections.

6.1 Geometry Importation

Specimen specific stem cross sectional geometries were extracted from rind boundaries of digitized plant specimens. In addition, vascular bundle boundaries were extracted from maize and sorghum specimens. The coordinates of the extracted boundaries were imported into FEA software to create models for analysis. The obtained coordinates were converted from pixel locations to world coordinates in units of millimeters. This unit conversion was done using the MATLAB `imref2D` function [55] and the calibration obtained during image acquisition. MATLAB scripts (pseudo code shown in Figure 6.1) were written to create the Python script files that are executed in Abaqus. In particular, the MATLAB code printed the command statements required to create a model, specify a sheet size, sketch splines, and rename sketches in Abaqus. The MATLAB code also printed the rind and vascular bundle spline coordinates. The Python script executed in Abaqus created a sketch as shown in Figure 6.2. Specific geometry importation protocols used for the plant species in this thesis can be found in Appendices A, B and C.

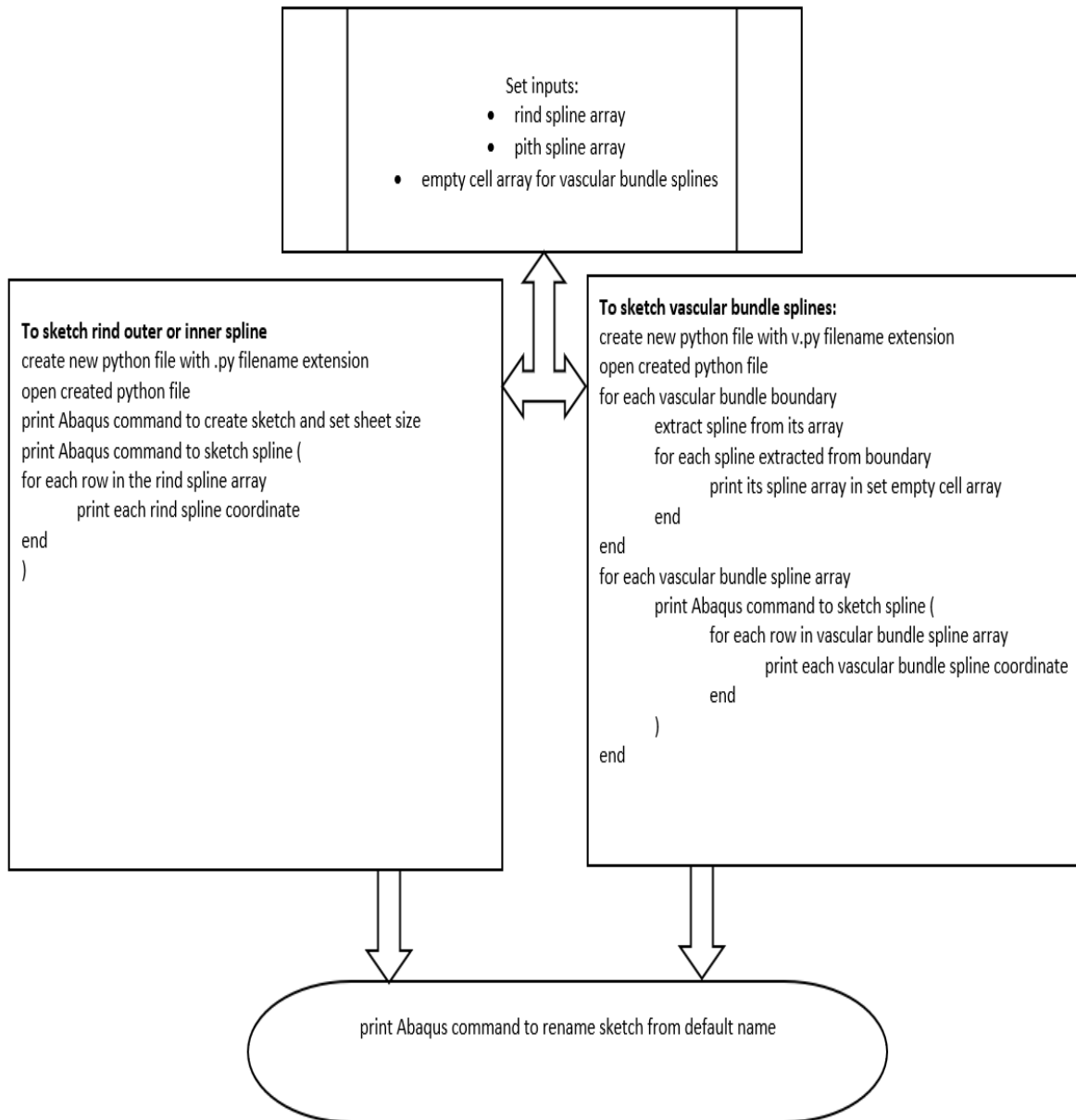


Figure 6.1: Pseudo code used to import geometry into third party software.

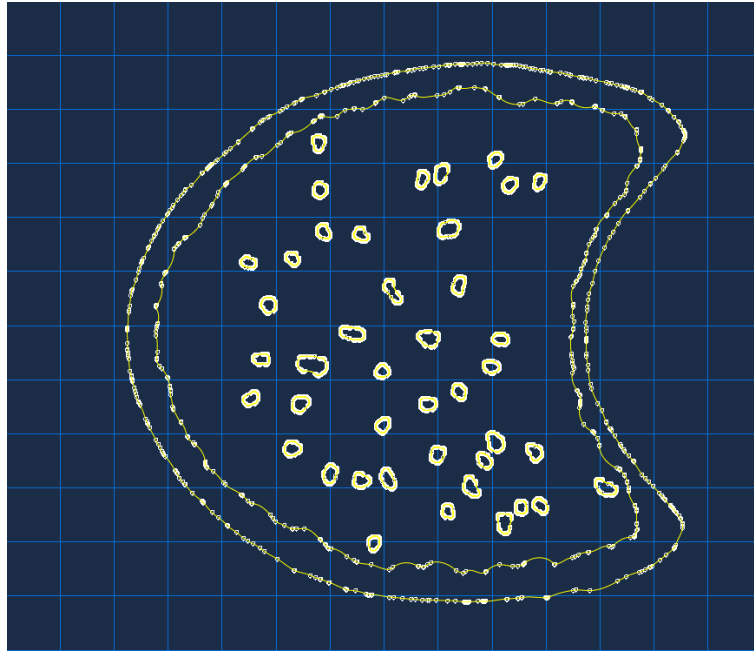


Figure 6.2: Imported maize stem specimen specific cross-sectional geometry.

6.2 Computer Modeling

Abaqus/CAE was used to develop the finite element models. Abaqus/standard was used to perform the finite element analysis. To create the computational model, the created Python script file was selected from its location folder and executed in Abaqus. Transverse compression and bending analysis were conducted to obtain the stiffness response of the stalk's internodes and locations of maximum stress along the stalk's internodes, respectively. Five internodes of a maize stalk were analyzed for their individual transverse stiffness. Bending analyses were performed on maize and wheat samples.

Specimen specific geometry was used to create two dimensional models. These models were subsequently subjected to transverse compression analyses. The maize stalk rind and pith materials were modeled as transversely isotropic. Documented material properties assigned were Young's modulus and Poisson's ratio. The average transverse Young's modulus of the rind and pith materials were set as 0.85GPa and 0.026GPa, respectively. While the Poisson's ration was set as 0.25 [59]. The structures were meshed at a global seed size of 0.2mm with four-node bilinear plane stress reduced

integration quadrilateral elements with hourglass control. Two platens were used, where the top platen was displaced downward at a maximum of 1mm for compression and fixed in the rotational and horizontal direction while the bottom platen was fixed in all degrees of freedom.

The reaction force of maize internodes subjected to compressive loading ranged between 15N and 18N. The reaction force increased from the bottom internodes to the top. The model's maximum stress under compression as seen in Figure 6.3 are concentrated around areas close to the platen for the bottom three internodes. However, the top two internodes which have a distinct cross section, show a different stress contour where the stress is distributed along the edges at the bottom of the major axis.

In addition to the previously mentioned compression analyses several models were created and subjected to bending loads. In particular, specimen specific geometry of maize and wheat samples were used to create three-dimensional models. The models were meshed with eight-node linear three-dimensional stress brick reduced integration hexahedral elements as shown in Figure 6.4 and Figure 6.5. One cross-sectional surface of the model was fixed in all degrees of freedom while bending moment was assigned to the other surface along the major axis direction (see Figure 6.6 and Figure 6.7). Low bending moment of 1Nm were applied to the maize and wheat model. Documented material properties of maize and wheat were assigned to the models. Young's modulus of 4.41GPa and 0.02GPa were assigned for rind and pith materials of maize respectively with a Poisson's ratio of 0.2 [58]. Young's modulus of 2.23GPa was assigned to the rind of the hollow wheat model with a Poisson's ratio of 0.413 [61].

The maximum stress experienced by the wheat stalk internode was 1.672MPa under a bending moment of 1Nm. The maize stalk internode experienced maximum stress of 0.09609MPa under a bending moment 1Nm. As can be seen in Figure 6.8 and 6.9 both models depict similar maximum stress locations along the length of the internode. The top and bottom surfaces of the internode's loading axis experience the maximum stresses.

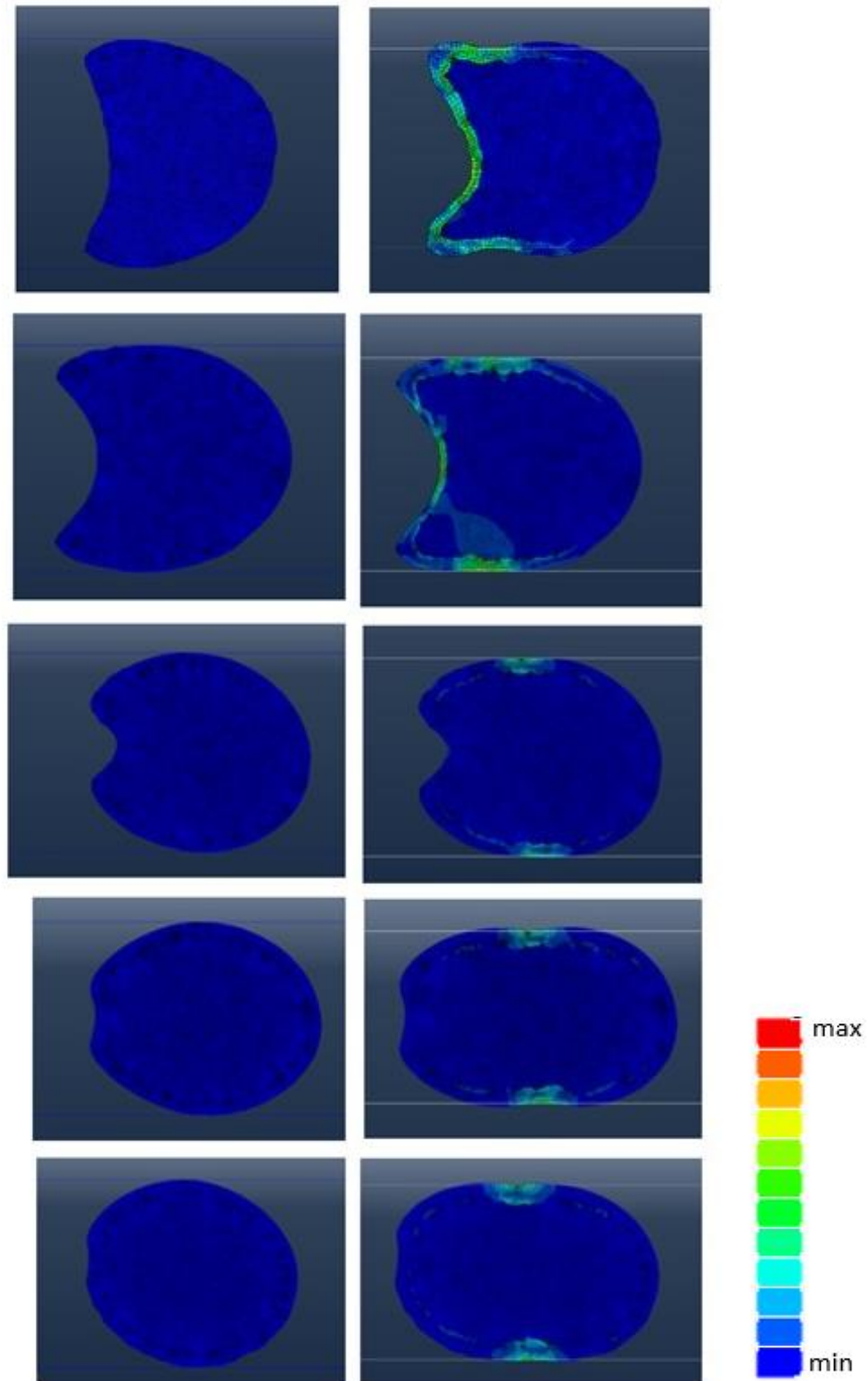


Figure 6.3: Undeformed (left) and Deformed (right) models of a maize stalk loaded in compression, showing Von Mises stress (MPa) experienced from the top internode (top) to the bottom internode (bottom).

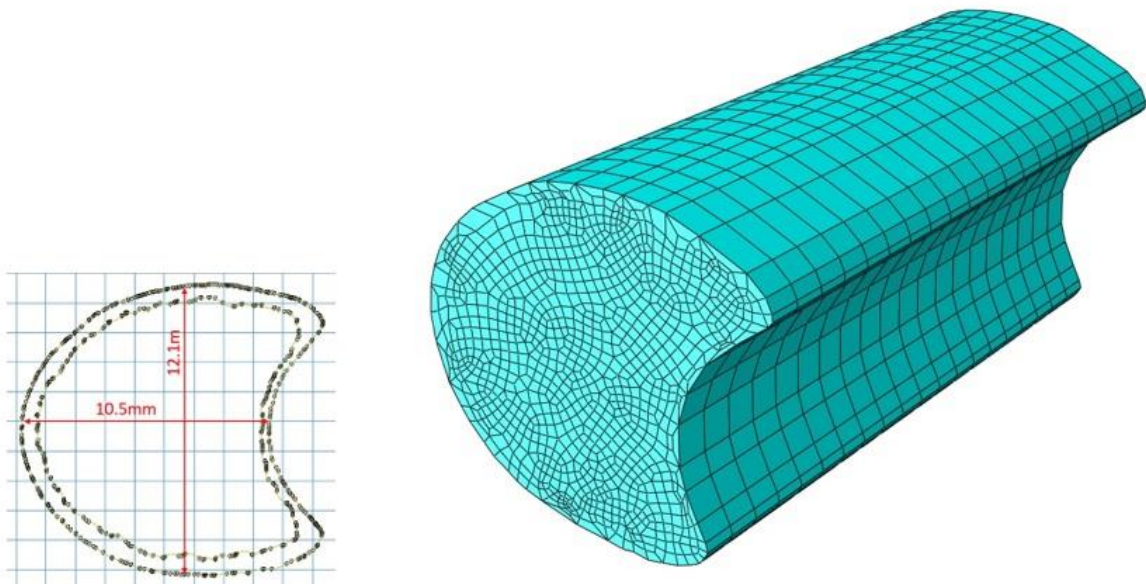


Figure 6.4: Undeformed three-dimensional model of maize stalk (right) and its cross-section (left).

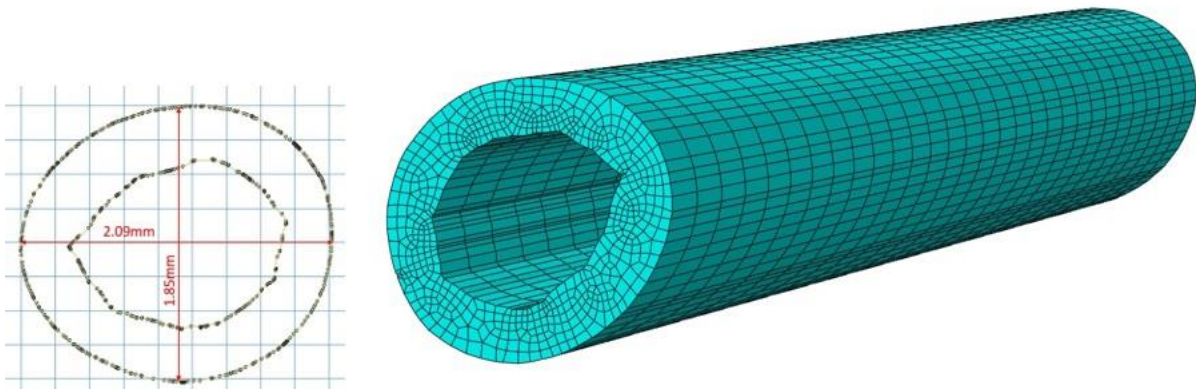


Figure 6.5: Undeformed three-dimensional model of wheat stalk (right) and its cross-section (left).

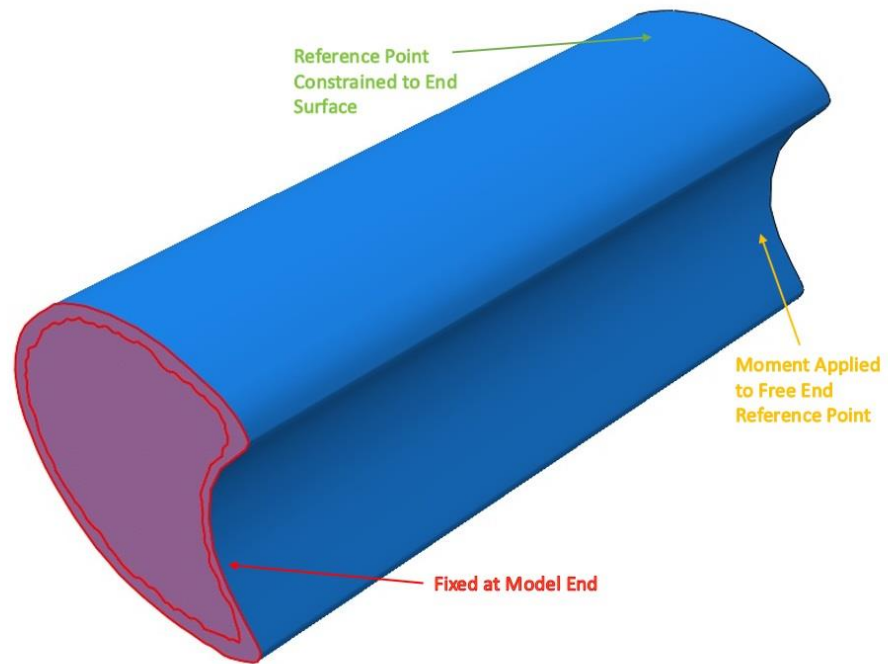


Figure 6.6: Boundary conditions and loads applied to maize stalk model.

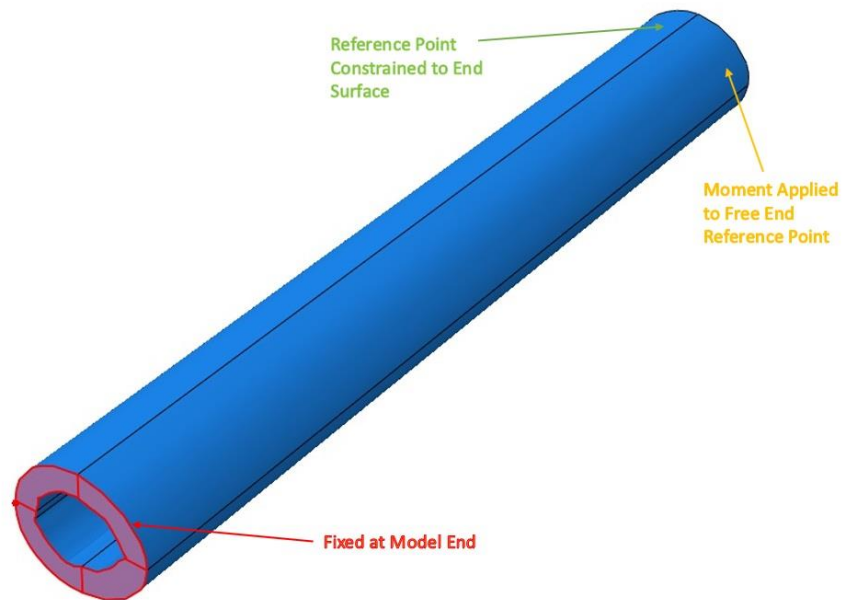


Figure 6.7: Boundary conditions and loads applied to wheat stalk model.

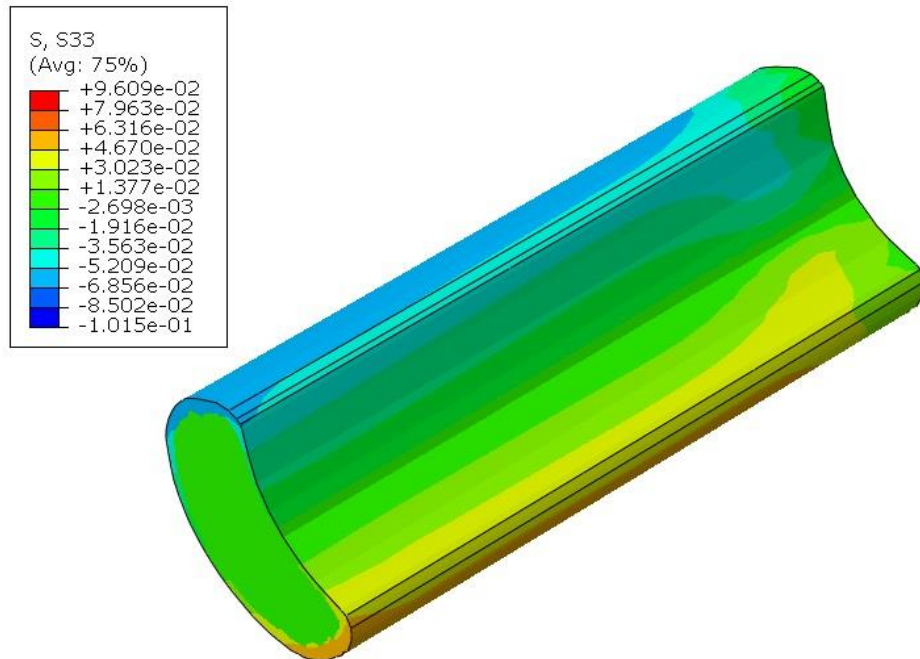


Figure 6.8: Deformed model of maize stalk internode under bending showing principal stress (MPa) contours along the stalk.

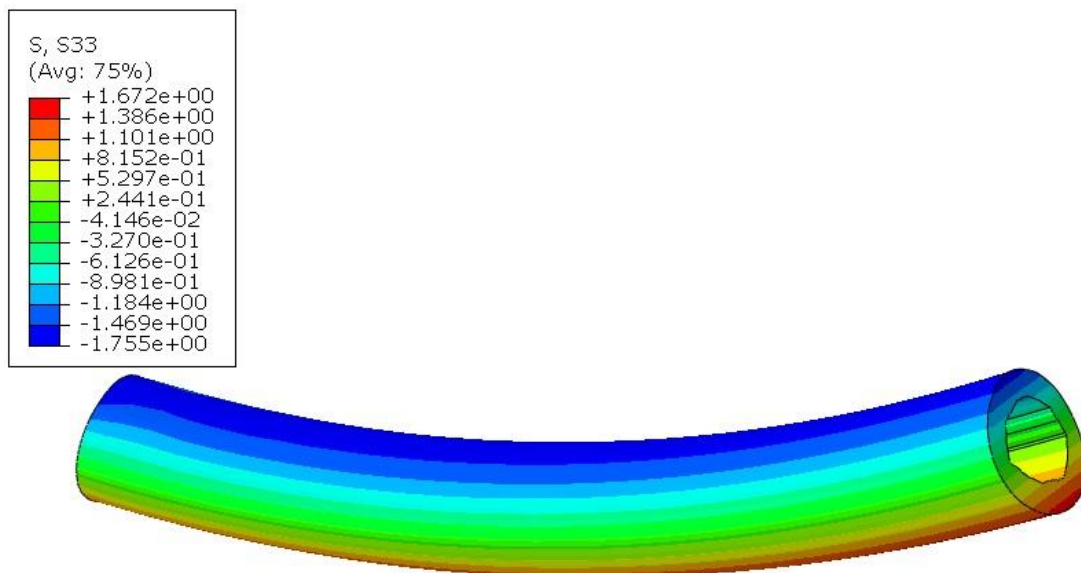


Figure 6.9: Deformed model of wheat stalk internode under bending showing principal stress (MPa) contours along the stalk.

Chapter 7: Conclusions, Recommendations, and Future Work

7.1 Conclusion

A fast, simple, and inexpensive methodology has been developed to extract quantitative phenotypes from plant stalks in a high throughput manner. A quick and simple sample preparation methodology was presented wherein thin 1-4mm sections of maize, poison hemlock, sorghum, wheat and Arabidopsis were produced. These sections were stained using an Alcian Blue-Safranin O staining sequence. Quality digitized images of stained specimens were obtained using a relatively inexpensive stereo microscope and 18MP camera. Digitized images were analyzed using an image processing algorithm developed in MATLAB to determine the major and minor diameter, rind thickness and number of vascular bundles in each image. The MATLAB algorithm was also used to import the extracted phenotypes from each image into a third-party finite element software for further biomechanical analysis. The importance of specimen specific geometry in producing computational models and performing finite element analysis was also illustrated.

7.2 Recommendations

There are three principal limitations in this study and each limitation is discussed in more details in paragraphs below. The first limitation was the ability of the image analysis program to automatically detect pith voids, the second limitation was related to staining procedures and the final limitation was related to developing FEA models.

Voids sometimes occur in the pith of pith filled plant species and with the current imaging algorithm its difficult to detect these voids automatically. These pith voids often prevented accurate image processing of stalk sections. The algorithm could be improved to enable detection of pith voids in plant cross sections in an automated manner.

There is little prior research on effectively staining mature dry plant samples. While the staining procedure developed as part of this thesis was effective it could be improved. For example, we found that stained plant sections produced unusual colors that were different from conventional stained sections. It is unclear what the cause of this was. But it is possible that through further research the contrast between plant structures of interest could be enhanced.

Computational models were assumed to be transversely isotropic in this study. This is because the principal purpose was to demonstrate that finite element models could be created from captured images. The models developed in this study should not be used to investigate complex biomechanical

phenomenon that require accurate material properties definition. Further research could be conducted to enable accurate examination of more complex models.

7.3 Future Work

The methodology developed as part of this thesis primarily enables phenotyping of stalk internode geometry. While the geometry of cross-sections along the length of stalk internodes are typically consistent, some internodes have a twisted configuration with significant angular rotations and diameter differences in successively cut internode slices. The nodes connecting internodes have also been reported as stress concentration areas. More research could be conducted to ensure accurate extraction of these geometry changes and subsequently more accurate computational modeling of plant stalks.

References

- [1] Niklas, K.J. and Spatz, H.C., 2012. *Plant Physics*. University of Chicago Press.
- [2] Geitmann, A., 2020. "Plant biomechanics—an interdisciplinary lens on plant biology." *Botany*, 98(1), pp.vii-viii.
- [3] Niklas, K.J., Spatz, H.C. and Vincent, J., 2006. "Plant biomechanics: an overview and prospectus." *American journal of botany*, 93(10), pp.1369-1378.
- [4] Geitmann, A., Niklas, K. and Speck, T., 2019. "Plant biomechanics in the 21st century." *Journal of Experimental Botany*, 70(14), pp. 3435-3438
- [5] Sudhakar, P., Latha, P. and Reddy P.V., 2016. *Phenotyping Crop Plants for Physiological and Biochemical Traits*. Academic Press.
- [6] European Plant Phenotyping Network. 2020. Why do we need plant phenotyping? [online] Available at: <https://www.plant-phenotyping-network.eu/> (Accessed on November 10, 2020)
- [6] Peltola, H.M., 2006. Mechanical stability of trees under static loads. *American journal of botany*, 93(10), pp.1501–1511.
- [7] Stubbs, C.J., Oduntan, Y.A., Keep, T.R., Noble, S.D. and Robertson, D.J., 2020. "The effect of plant weight on estimations of stalk lodging resistance." *Plant methods*, 16(1), pp.1-18.
- [8] Awika, J. M., 2011. "Major Cereal Grains Production and Use around the World." In *Advances in Cereal Science: Implications to Food Processing and Health Promotion*, edited by Awika, J. M., Piironen, V., and Bean, S., 1089, Chap. 1 pp.1–13. ACS Symposium Series. Washington, DC.
- [9] Edgerton M. D. 2009. "Increasing crop productivity to meet global needs for feed, food, and fuel." *Plant physiology*, 149(1), pp.7–13.
- [10] Flint-Garcia and Sherry A. 2003. "Quantitative Trait Locus Analysis of Stalk Strength in Four Maize Populations." *Crop science*, 43(1), pp.13-22.
- [11] Golden Harvest. 2020. Late Season Wind Damage Impacts Maize Yield. [online] Available at: <https://www.goldenharvestseeds.com/agronomy/articles/late-season-wind-damage-impacts-maize-yield> (Accessed on November 10, 2020)

- [12] Shah, D.U., Reynolds, T.P. and Ramage, M.H., 2017. "The strength of plants: theory and experimental methods to measure the mechanical properties of stems." *Journal of Experimental Botany*, 68(16), pp.4497-4516.
- [13] Seegmiller, W. 2020. "A Novel Puncture Method for Determining Plant Stem Morphology and Lodging Resistance." M.S thesis, Idaho, ID: University of Idaho.
- [14] Yeung, E.C., 1999. "The use of histology in the study of plant tissue culture systems—some practical comments." *In Vitro Cellular & Developmental Biology-Plant*, 35(2), pp.137-143.
- [15] Ruzin, S.E., 1999. *Plant microtechnique and microscopy* (Vol. 198). New York: Oxford University Press.
- [16] Soukup, A. and Tylová, E., 2014. Essential methods of plant sample preparation for light microscopy. *Plant Cell Morphogenesis*. Humana Press, Totowa, NJ. Chap. 1, pp. 1-23.
- [17] Nebesářová, J., 2019. Essential Methods of Plant Sample Preparation for High-Resolution Scanning Electron Microscopy at Room Temperature. *Plant Cell Morphogenesis*, 2nd ed., Humana, New York, NY. Chap. 4, pp. 63-76.
- [18] Sathananthan, A.H. and Nottola, S.A., 2007. Digital imaging of stem cells by electron microscopy. *Stem Cell Assays*. Humana Press. Chap. 3, pp. 21-41.
- [19] Verhertbruggen, Y., Walker, J.L., Guillon, F. and Scheller, H.V., 2017. A comparative study of sample preparation for staining and immunodetection of plant cell walls by light microscopy. *Frontiers in plant science*, 8, p.1505.
- [20] Pathan, A.K., Bond, J. and Gaskin, R.E., 2010. "Sample preparation for SEM of plant surfaces." *Materials Today*, 12 (1), pp.32-43.
- [21] Du, J., Zhang, Y., Guo, X., Ma, L., Shao, M., Pan, X. and Zhao, C., 2017. "Micron-scale phenotyping quantification and three-dimensional microstructure reconstruction of vascular bundles within maize stalks based on micro-CT scanning." *Functional Plant Biology*, 44(1), pp.10-22.
- [22] Hesse, L., Bunk, K., Leupold, J., Speck, T. and Masselter, T., 2019. "Structural and functional imaging of large and opaque plant specimens." *Journal of experimental botany*, 70(14), pp.3659-3678.

- [23] Schubert, V., 2017. "Super-resolution microscopy—applications in plant cell research." *Frontiers in plant science*, 8, p.531.
- [24] Biosystems Switzerland AG. 2020. Leica VT1200 S fully automated vibrating blade microtome.[online] Available at: <https://biosystems.ch/default.aspx?globalid=3525&lang=EN> (Accessed on November 14, 2020)
- [25] Leica Biosystems Nussloch. 2020. Leica Biosystems RM2245 Semi-Automated Rotary Microtome. [online] Available at: <https://www.leicabiosystems.com/histology-equipment/microtomes/products/leica-rm2245/> (Accessed on November 14, 2020)
- [26] Leica Biosystems. (2020). Sliding Microtome [online] Available at: <https://www.leicabiosystems.com/histology-equipment/sliding-and-vibrating-blade-microtomes/> (accessed on: October 27, 2020)
- [27] Bruker. (2020). Microtomography [online]. Available at: <https://www.bruker.com/products/microtomography/in-vivo-micro.html> (Accessed on: October 27, 2020)
- [28] Bruker. (2020). Magnetic Resonance-Preclinical MRI-BioSpec [online]. Available at: <https://www.bruker.com/nc/products/mr/preclinical-mri/biospec.html> (accessed on October 27, 2020)
- [29] Lab Manager. (2020). Business Management-Buying a SEM. [blog]. Available at: <https://www.labmanager.com/business-management/buying-a-pre-owned-sem-19283> (Accessed on October 27, 2020)
- [30] Micro Photonics Inc. (2015). How much does a Micro-CT Scanner Cost? [blog]. Available at: <https://www.microphotonics.com/how-much-does-a-micro-ct-scanner-cost/> (Accessed on October 27, 2020)
- [31] Amscope. (2020). Stereo Microscopes. [online]. Available at: <https://www.amscope.com/stereo-microscopes.html> (Accessed on October 27, 2020)
- [32] JOEL Ltd. (2020). JSM-7610F Schottky Field Emission Scanning Electron Microscope [online]. Available at: <https://www.jeol.co.jp/en/products/detail/JSM->

- 7610F.html#:~:text=JSM%2D7610F%20is%20an%20ultra,for%20high%20spatial%20resolutio
n%20analysis. (Accessed on November 14, 2020)
- [33] Baker Hughes Company. (2020). Phoenix nanotom m 3d metrology nano ct [online]. Available at: <https://www.bakerhughesds.com/industrial-x-ray-ct-scanners/phoenix-nanotom-m-3d-metrology-nano-ct> (Accessed on November 14, 2020)
- [34] Bruker. (2020). BioSpec 117/16 [online]. Available at: <https://www.bruker.com/products/mr/preclinical-mri/biospec-11716.html> (Accessed on November 14, 2020)
- [35] Yang, W., Feng, H., Zhang, X., Zhang, J., Doonan, J.H., Batchelor, W.D., Xiong, L. and Yan, J., 2020. "Crop phenomics and high-throughput phenotyping: past decades, current challenges, and future perspectives." *Molecular Plant*, 13(2), pp.187-214.
- [36] Rahaman, M., Chen, D., Gillani, Z., Klukas, C. and Chen, M., 2015. "Advanced phenotyping and phenotype data analysis for the study of plant growth and development." *Frontiers in plant science*, 6, p.619.
- [37] Perez-Sanz, F., Navarro, P.J. and Egea-Cortines, M., 2017. "Plant phenomics: an overview of image acquisition technologies and image data analysis algorithms." *GigaScience*, 6(11), p.gix092.
- [38] Dhondt, S., Wuyts, N. and Inzé, D., 2013. "Cell to whole-plant phenotyping: the best is yet to come." *Trends in plant science*, 18(8), pp.428-439.
- [39] van Dusschoten, D., Metzner, R., Kochs, J., Postma, J.A., Pflugfelder, D., Bühler, J., Schurr, U. and Jahnke, S., 2016. "Quantitative 3D analysis of plant roots growing in soil using magnetic resonance imaging." *Plant physiology*, 170(3), pp.1176-1188.
- [40] Mairhofer, S., Zappala, S., Tracy, S.R., Sturrock, C., Bennett, M., Mooney, S.J. and Pridmore, T., 2012. "RooTrak: automated recovery of three-dimensional plant root architecture in soil from X-ray microcomputed tomography images using visual tracking." *Plant physiology*, 158(2), pp.561-569.
- [41] Fiorani, F. and Schurr, U., 2013. "Future scenarios for plant phenotyping." *Annual review of plant biology*, 64, pp.267-291.

- [42] Li, L., Zhang, Q. and Huang, D., 2014. "A review of imaging techniques for plant phenotyping." *Sensors*, 14(11), pp.20078-20111.
- [43] Zhang, Y. and Zhang, N., 2018. "Imaging technologies for plant high-throughput phenotyping: A review." *Front. Agric. Sci. Eng*, 5, pp.406-419.
- [44] Tardieu, F., Cabrera-Bosquet, L., Pridmore, T. and Bennett, M., 2017. "Plant phenomics, from sensors to knowledge." *Current Biology*, 27(15), pp.R770-R783.
- [45] Zhang, Y., Legay, S., Barrière, Y., Méchin, V. and Legland, D., 2013. "Color quantification of stained maize stem section describes lignin spatial distribution within the whole stem." *Journal of agricultural and food chemistry*, 61(13), pp.3186-3192.
- [46] Legland, D., Devaux, M.F. and Guillon, F., 2014. "Statistical mapping of maize bundle intensity at the stem scale using spatial normalisation of replicated images." *PLoS One*, 9(3), p.e90673.
- [47] Legland, D., El-Hage, F., Méchin, V. and Reymond, M., 2017. "Histological quantification of maize stem sections from FASGA-stained images." *Plant Methods*, 13(1), p.84.
- [48] Heckwolf, S., Heckwolf, M., Kaeppler, S.M., de Leon, N. and Spalding, E.P., 2015. "Image analysis of anatomical traits in stalk transections of maize and other grasses." *Plant Methods*, 11(1), pp.1-11.
- [49] Zhang, Y., Ma, L., Pan, X., Wang, J., Guo, X. and Du, J., 2018. "Micron-scale phenotyping techniques of maize vascular bundles based on X-ray microcomputed tomography." *JoVE (Journal of Visualized Experiments)*, (140), p.e58501.
- [50] Ives, E., 2001. *A guide to wood microtomy: Making quality microslides of wood sections*. Ernie Ives.
- [51] Parker, A.J., Haskins, E.F. and Deyrup-Olsen, I., 1982. Toluidine blue: a simple, effective stain for plant tissues. *The American Biology Teacher*, 44(8), pp.487-489.
- [52] Bradley, D. and Roth, G., 2007. Adaptive thresholding using the integral image. *Journal of graphics tools*, 12(2), pp.13-21.
- [53] Otsu, N., 1979. A threshold selection method from gray-level histograms. *IEEE transactions on systems, man, and cybernetics*, 9(1), pp.62-66.

- [54] Van Den Boomgaard, R. and Van Balen, R., 1992. Methods for fast morphological image transforms using bitmapped binary images. *CVGIP: Graphical Models and Image Processing*, 54(3), pp.252-258.
- [55] MATLAB. 2019. version 9.6.0 1072779 (R2019a). The MathWorks Inc. Natick, Massachusetts.
- [56] Stubbs, Christopher J. 2019. "Computational modeling of maize stems". New York, NY: New York University.
- [57] Stubbs, C.J., Baban, N.S., Robertson, D.J., Alzube, L. and Cook, D.D., 2018. Bending stress in plant stems: models and assumptions. In *Plant Biomechanics* (pp. 49-77). Springer, Cham.
- [58] Forell, G.V., Robertson, D., Lee, S.Y. and Cook, D.D., 2015. Preventing lodging in bioenergy crops: a biomechanical analysis of maize stalks suggests a new approach. *Journal of experimental botany*, 66(14), pp.4367-4371.
- [59] Stubbs, C.J., Sun, W. and Cook, D.D., 2019. "Measuring the transverse Young's modulus of maize rind and pith tissues." *Journal of biomechanics*, 84, pp.113-120.
- [60] Robertson, D.J., Julias, M., Gardunia, B.W., Barten, T. and Cook, D.D., 2015. "Maize stalk lodging: a forensic engineering approach provides insights into failure patterns and mechanisms." *Crop Science*, 55(6), pp.2833-2841.
- [61] Li, L. and Yuming, G., 2008. "Analysis and Finite Element Simulation for mechanical response of wheat under wind and rain loads." *International Journal of Agricultural and Biological Engineering*, 1(1), pp.82-88.

Appendix A: Protocol for Phenotyping Maize or Sorghum Stalks

Sectioning

- Identify stalks to section. Label each internode and take morphological measurements of internodes including length, major diameter, and minor diameter if necessary. Record these measurements and stalk labels appropriately for subsequent reference.
- Cut the whole stalk into internodal segments. Set the trim saw blade speed to a low setting of 2 and if required (for stronger stalks) increase to 3 or 4.
- Cut internode segments into slices. Hold internode segments firmly with saw vise and adjust saw fence according to required thickness. Best thickness for slices is 2-4mm. Have a bag or Ziplock for storing each internode's slices.

Staining

- Prepare stain solutions. Alcian Blue solution can be made by mixing 3grams of Alcian Blue, 250ml of distilled water, 6 drops of glacial acetic acid and 4ml of formaldehyde 40% solution. Safranin O Solution can be made by mixing 3grams of Safranin O, 100ml of Methylated Spirit, 100ml of distilled water and 2ml of formaldehyde 40% solution. Prepare stain solutions and keep for at least a day before use. Stain solutions can be stored and used for up to 6 months.
- Prepare slices for staining. Disposable cups can be used for staining. Punch holes in two cups to enable easy flow of liquid. One cup holds the slices and the other prevents them from floating while staining.
- Hydrate slices in distilled water for 5minutes.
- Stain samples in Alcian Blue solution for 20minutes .
- Rinse slices quickly in distilled water for 1minute.
- Stain samples in Safranin O for 1 hour.
- Rinse slices quickly in distilled water for 1minute.
- Dehydrate slices in alcohol for 2minutes.
- Mount slices for imaging.

Imaging

- Prepare stereoscope and AmScope software for imaging. Connect camera to computer. Run camera software. Click on camera from camera list. Create folders for batch saving each image of internode's slices. Save images in tagged image file (tif) format.
- Calibrate stereoscope. Set the stereoscope to an adequate height, attach the 0.5X Barlow lens to stereoscope and adjust the camera appropriately to ensure sharp, quality images can be captured. Calibrate according to stereoscope manual. Record calibration factor for image processing.
- Capture images of stained slices and save accordingly.

Image Processing

- Open MATLAB and run algorithm.
- Assign input parameters in algorithm. Set folders where images would be read from and created files would be saved into. Set calibration factor.
- Run the algorithm. Images are automatically read in and files are automatically saved in set folders.

Geometry importation

- Run Abaqus and open a new file. Set working directory to where created files can be read from.
- Run scripts in Abaqus. Select created python files for slice rind splines. Selected files are executed in Abaqus and geometry sketches are created.
- Continue producing computational model accordingly.

Appendix B: Protocol for Phenotyping Poison Hemlock Stalks

Sectioning

- Identify stalks to section. Label each internode and take morphological measurements of internodes including length, major diameter, and minor diameter if necessary. Record these measurements and stalk labels appropriately for subsequent reference.
- Cut the whole stalk into internodal segments. Set the trim saw blade speed to a low setting of 2 and if required (for stronger stalks) increase to 3 or 4.
- Cut internode segments into slices. Hold internode segments firmly with saw vise and adjust saw fence according to required thickness. Best thickness for slices is 2-4mm. Have a bag or Ziplock for storing each internode's slices.

Staining

- Prepare stain solutions. Alcian Blue solution can be made by mixing 3grams of Alcian Blue, 250ml of distilled water, 6 drops of glacial acetic acid and 4ml of formaldehyde 40% solution. Safranin O Solution can be made by mixing 3grams of Safranin O, 100ml of Methylated Spirit, 100ml of distilled water and 2ml of formaldehyde 40% solution. Prepare stain solutions and keep for at least a day before use. Stain solutions can be stored and used for up to 6 months.
- Prepare slices for staining. Disposable cups can be used for staining. Punch holes in two cups to enable easy flow of liquid. One cup holds the slices and the other prevents them from floating while staining.
- Hydrate slices in distilled water for 5minutes.
- Stain samples in Alcian Blue solution for 20minutes .
- Rinse slices quickly in distilled water for 1minute.
- Stain samples in Safranin O for 1 hour.
- Rinse slices quickly in distilled water for 1minute.
- Dehydrate slices in alcohol for 2minutes.
- Mount slices for imaging.

Imaging

- Prepare stereoscope and AmScope software for imaging. Connect camera to computer. Run camera software. Click on camera from camera list. Create folders for batch saving each image of internode's slices. Save images in tagged image file (tif) format.
- Calibrate stereoscope. Set the stereoscope to an adequate height, attach the 0.5X Barlow lens to stereoscope and adjust the camera appropriately to ensure sharp, quality images can be captured. Calibrate according to stereoscope manual. Record calibration factor for image processing.

Image Processing

- Open MATLAB and run algorithm.
- Assign input parameters in algorithm. Set folders where images would be read from and created files would be saved into. Set calibration factor.
- Run the algorithm. Images are automatically read in and files are automatically saved in set folders.

Geometry importation

- Run Abaqus and open a new file. Set working directory to where created files can be read from.
- Run scripts in Abaqus. Select created python files for slice rind, pith and vascular bundle splines. Selected files are executed in Abaqus and geometry sketches are created.
- Continue producing computational model accordingly.

Appendix C: Protocol for Phenotyping Wheat and Arabidopsis Stalks

Sectioning

- Identify stalks to section. Label each internode and take morphological measurements of internodes including length, major diameter, and minor diameter if necessary. Record these. Label stalks appropriately for subsequent reference.
- Cut the whole stalk into internodal segments. Use a razor blade to cut stalks into different segments.
- Prepare segments for cutting. Hydrate segments in distilled water for few minutes.
- Cut internode segments into slices. Hold internode firmly in one hand with thumb and index finger and cut with other hand. Hold blade perpendicular to internode and create slices simultaneously by drawing razor blade through sample. Best thickness for slices is 1-2mm. Have a bag or Ziplock for storing each internode's slices.

Staining

- Prepare stain solutions. Alcian Blue solution can be made by mixing 3grams of Alcian Blue, 250ml of distilled water, 6 drops of glacial acetic acid and 4ml of formaldehyde 40% solution. Safranin O Solution can be made by mixing 3grams of Safranin O, 100ml of Methylated Spirit, 100ml of distilled water and 2ml of formaldehyde 40% solution. Prepare stain solutions and keep for at least a day before use. Stain solutions can be stored and used for up to 6 months.
- Prepare slices for staining. Disposable cups can be used for staining. Punch holes in two cups to enable easy flow of liquid. One cup holds the slices and the other prevents them from floating.
- Hydrate slices in distilled water for 5minutes.
- Stain samples in Alcian Blue solution for 20minutes .
- Rinse slices quickly in distilled water for 1minute.
- Stain samples in Safranin O for 1 hour.
- Rinse slices quickly in distilled water for 1minute.
- Dehydrate slices in alcohol for 2minutes.
- Mount slices for imaging.

Imaging

- Prepare stereoscope and AmScope software for imaging. Connect camera to computer. Run camera software. Click on camera from camera list. Create folders for batch saving each image of internode's slices. Save images in tagged image file (tif) format.
- Calibrate stereoscope. Set the stereoscope to an adequate height, attach the 2.0X Barlow lens to stereoscope and adjust the camera appropriately to ensure sharp, quality images can be captured. Calibrate according to stereoscope manual. Record calibration factor for image processing.

Image Processing

- Open MATLAB and run algorithm.
- Assign input parameters. Set folders where images would be read from and created files would be saved into. Set calibration factor.
- Run the algorithm. Images are automatically read in and files are automatically saved in set folders.

Geometry importation

- Run Abaqus and open a new file. Set working directory to where created files can be read from.
- Run scripts in Abaqus. Select created python files for slice rind splines. Selected files are executed in Abaqus and geometry sketches are created.
- Continue producing computational model accordingly.

Appendix D: MATLAB Code for the Image Processing of Maize and Sorghum Stalks.

```

%% automatically extract rind and pith splines, find rind thickness, major and minor diameter, and
number of vascular bundles in a stained sample.

%% assigned variables list
%% a – raw magnified image
%% s – calibration factor
%% rs – coordinates of rind boundary in mm
%% ps – coordinates of pith boundary in mm
%% rthickness – rind thickness in mm
%% C – rind centroid
%% Major_D – major diameter
%% Minor_D – minor diameter
%% no_vbundles – number of vascular bundles

myfolder='C:\Users\odun3492\Documents\U Drive\Modeling\fns\splines\m\test'; % insert address
of folder containing sample images
filepattern=fullfile(myfolder,'*.tif');
thefiles=dir(filepattern);
for i=1:length(thefiles)
    basefilename=thefiles(i).name;
    fullfilename=fullfile(thefiles(i).folder,basefilename);

%% get inner and outer boundary of rind
a=imread(fullfilename); % read image from folder into matlab
ag=rgb2gray(a); % convert color image to grayscale
at=adaptthresh(ag,0.8); % obtain a suitable threshold value for binarizing image
ab=imbinarize(ag,at); % binarize imported image
ab1=bwareafilt(ab,1); % extract the biggest object (rind) from the binary image
ao=~ab1; % give the complement of the extracted rind
ao1=bwareafilt(ao,1); % extract the biggest object (rind) from the complemented image
aof=imfill(ao1,'holes'); % fill the holes in rind image

```

```

rb=bwboundaries(aof); % trace the boundaries of the rind and extract coordinates (in cell format)
rb=rb{1}; % extract boundary coordinates from cell
urb=unique(rb(:,1:2),'rows','stable'); % remove repeated rind boundary coordiantes
xi=urb(:,2); % x-coordinates of rind boundary
yi=urb(:,1); % y-coordinates of rind boundary
rb2=boundary(xi,yi); % extract spline from rind boundary coordinates
rx=xi(rb2); % x-coordinates of rind spline
ry=yi(rb2); % y-coordinates of rind spline
osp=[ry,rx]; % rind spline coordinates
s=1/175; % calibration factor
Ro=imref2d(size(aof),s,s);
for i=1:1:length(osp)
    [rs(i,2),rs(i,1)] = intrinsicToWorld(Ro,osp(i,2),osp(i,1)); % convert rind coordinates to mm
end

abc=imclearborder(ab); % remove the rind from the binary image
abc1=bwareafilt(abc,1); % extract the pith from the binary image
se=strel('disk',10); % create an object used to remove noise from image
ai=imclose(abc1,se); % remove noise from pith using objects created
ai=imfill(ai,'holes'); % fill holes in pith
pb=bwboundaries(ai);
pb=pb{1};
upb=unique(pb(:,1:2),'rows','stable');
xi=upb(:,2);
yi=upb(:,1);
pb2=boundary(xi,yi);
px=xi(pb2);
py=yi(pb2);
isp=[py,px];
Ri=imref2d(size(ai),s,s);
for i=1:1:length(isp)
    [ps(i,2),ps(i,1)] = intrinsicToWorld(Ri,isp(i,2),isp(i,1));
end

```

```

rsx=rs(:,2); % x-coordinates of rind spline in mm
rsy=rs(:,1); % y-coordinates of rind spline in mm
psx=ps(:,2); % x-coordinates of pith spline in mm
psy=ps(:,1); % y-coordinates of pith spline in mm
ospl=length(osp);% number of rind spline coordinates
rsl=length(rs); % number of rind spline coordinates after conversion to mm
rsxx=rsl-ospl; % check to make sure number of converted coordinates are similar to original
rsr=rsl-(rsxx-1); % check to see if conversion increases coordinates
if rsxx~=0
    rs(rsr:end,:)=[]; % delete extra coordinates created from conversion
end
ispl=length(isp);
psl=length(ps);
psxx=psl-ispl;
psr=psl-(psxx-1);
if psxx~=0
    ps(psr:end,:)=[];
end
rsx=rs(:,2); % final x-coordinates of rind spline in mm
rsy=rs(:,1); % final y-coordinates of rind spline in mm
psx=ps(:,2); % final x-coordinates of pith spline in mm
psy=ps(:,1); % final y-coordinates of pith spline in mm
%% % plot extracted rind and pith splines
axis('on')
plot(rsx,rsy,psx,psy)
set(gca,'YDir','reverse'); % reverse y-axis in order to get correct orientation of splines

%% % find the rind thickness of the sample
[dist,S]=pdist2(ps,rs,'euclidean','Smallest',1); % find the shortest pairwise distance between
coordinates of the inner and outer boundary and their indices
rthickness=mean(dist); % calculate the mean of the smallest distances to obtain rind thickness

```

```

rt_ips=ps(S,:); % using the indices obtained identify the inner boundary coordinates corresponding
to the shortest distance from the outer boundary
rt_xi=rt_ips(:,2); % x-coordinate of shortest distance
rt_yi=rt_ips(:,1); % y-coordinate of shortest distance

%% % find the major and minor diameter of the sample
C=regionprops(aof,'Centroid'); % find the centroid of the rind boundary
Cxy=cat(1,C.Centroid); % convert the centroid obtained into a matrix
Cx=Cxy(:,1); % x-coordinate of the centroid
Cy=Cxy(:,2); % y-coordinate of the centroid
[xc,yc]=intrinsicToWorld(Ri,Cx,Cy); % convert centroid coordinates to mm
hold on
plot(xc,yc,'+'); % plot centroid coordinates
Cx=int16(Cx); % convert x coordinate of centroid to whole number
Cy=int16(Cy); % convert y coordinate of centroid to whole number
xcl=aof(:,Cx); % extract vertical column from outer boundary matrix using centroid x-coordinate
ycl=aof(Cy,:); % extract horizontal row from outer boundary matrix using centroid y-coordinate
xc_f=find(xcl,1,'first'); % find top coordinate of vertical centre line
xc_l=find(xcl,1,'last'); % find bottom coordinate of vertical centre line
yc_f=find(ycl,1,'first'); % find first(left) coordinate of horizontal centre line
yc_l=find(ycl,1,'last'); % find last (right) coordinate of horizontal centre line
[xc_t,xc_b]=intrinsicToWorld(Ri,xc_f,xc_l);
[yc_le,yc_r]=intrinsicToWorld(Ri,yc_f,yc_l);
hold on
plot([xc,xc],[xc_t,xc_b]); % plot vertical centre line
plot([yc_le,yc_r],[yc,yc]); % plot horizontal centre line
Major_D=xc_b-xc_t; % obtain major diameter
Minor_D=yc_r-yc_le; % obtain minor diameter

%% % find the number of vascular bundles in sample
se1=strel('disk',13);
av=imclose(abc1,se1);

```

```

av1=~av;
av2=bwareafilt(av1,1);
avb=av1&~av2;
avb=bwareafilt(avb,[2000 10000]);
avbb=bwboundaries(avb); % find boundaries of blobs
no_vbundles=length(avbb); % obtain the number of vascular bundles

%%% write rind spline
spline = rs; %set inner or outer boundary
j='r';
filename = sprintf('%s%s.py',j,basefilename);
fileID = fopen(filename,'w'); %start a new text file
fprintf(fileID,'from sketch import *\n\n'); %'\n' means go to the next line
fprintf(fileID,'mdb.models["Model-1"].ConstrainedSketch(name="__profile__",
sheetSize=200.0)\n'); %print header information
fprintf(fileID,'mdb.models["Model-1"].sketches["__profile__"].Spline(points=(\n\t');
for i = 1:1:size(spline,1)
    formatSpec = '(%4.4f, %4.4f), ';
    fprintf(fileID,formatSpec,spline(i,1),spline(i,2));
end %run through each row and print it to the file
formatSpec = '(%4.4f, %4.4f)\n';
fprintf(fileID,formatSpec,spline(1,1),spline(1,2)); %re-print first data point to close the spline
fprintf(fileID,'\t)\n'); %print footer information
fprintf(fileID,'mdb.models["Model-1"].sketches.changeKey(fromName="__profile__",
toName="rindspline")\n');

%%% write pith spline
splinee = ps; %set inner or outer boundary
v='p';
filename = sprintf('%s%s.py',v,basefilename);
fileID = fopen(filename,'w'); %start a new text file
fprintf(fileID,'from sketch import *\n\n'); %'\n' means go to the next line

```

```

fprintf(fileID,'mdb.models["Model-1"].ConstrainedSketch(name="__profile__",
sheetSize=200.0)\n'); %print header information
fprintf(fileID,'mdb.models["Model-1"].sketches["__profile__"].Spline(points=(\n\t');
for i = 1:1:size(splinee,1)
    formatSpec = '(%4.4f, %4.4f), ';
    fprintf(fileID,formatSpec,splinee(i,1),splinee(i,2));
end %run through each row and print it to the file
formatSpec = '(%4.4f, %4.4f)\n';
fprintf(fileID,formatSpec,splinee(1,1),splinee(1,2)); %re-print first data point to close the spline
fprintf(fileID,'\t)\n'); %print footer information
fprintf(fileID,'mdb.models["Model-1"].sketches.changeKey(fromName="__profile__",
toName="pithspline")\n');

%%% write vascular bundle splines
h=cell(size(avbb));
q='vb';
filename = sprintf('%s%s.py',q,basefilename);
fileID = fopen(filename,'w'); %start a new text file
fprintf(fileID,'from sketch import *\n\n'); %'\n' means go to the next line
fprintf(fileID,'mdb.models["Model-1"].ConstrainedSketch(name="__profile__",
sheetSize=200.0)\n'); %print header information
for y=1:length(avbb)
    z=avbb{y};
    uz=unique(z(:,1:2),'rows','stable');
    uzx=uz(:,2);
    uzy=uz(:,1);
    z2=boundary(uzx,uzy);
    nzx=uzx(z2);
    nzy=uzy(z2);
    nz=[nzy*s,nzx*s];
    for s=1:1:length(h)
        h{y}=nz;

```

```
end
end
for k3=1:length(h) %
    bd3=h{k3};
    fprintf(fileID,'mdb.models["Model-1"].sketches["__profile__"].Spline(points=(\n\t');
    for n=1:1:size(bd3)
        formatSpec = '%4.4f, %4.4f, ';
        fprintf(fileID,formatSpec,bd3(n,1),bd3(n,2));
    end
    fprintf(fileID,'\t))\n');
end
fprintf(fileID,'mdb.models["Model-1"].sketches.changeKey(fromName="__profile__",
toName="vbspline")\n');
path=strcat('C:\Users\odun3492\Documents\U
Drive\Modeling\fns\splines\m\test\savesp\',basefilename); % insert address of folder where you
intend to save plots
saveas(gcf,path)
save(sprintf('%s.mat',basefilename),'rthickness','Major_D','Minor_D','no_vbundles') % this saves
in current matlab folder
close all
end
```


Appendix E: MATLAB Code for the Image Processing of Wheat, Poison Hemlock and Arabidopsis Stalks.

```

%% automatically extract rind splines, find rind thickness, major and minor diameter in a stained
hollow sample

%% assigned variables list
%% a – raw magnified image
%% s – calibration factor
%% rs – coordinates of rind outer boundary in mm
%% ps – coordinates of inner boundary in mm
%% rthickness – rind thickness in mm
%% C – rind centroid
%% Major_D – major diameter
%% Minor_D – minor diameter

myfolder='C:\Users\odun3492\Documents\U Drive\Modeling\fns\splines\w\test'; % insert address
of folder containing sample images
filepattern=fullfile(myfolder,'*.tif');
thefiles=dir(filepattern);
for i=1:length(thefiles)
    basefilename=thefiles(i).name;
    fullfilename=fullfile(thefiles(i).folder,basefilename);
    a=imread(fullfilename); % read image into matlab

    %% segment image by rgb layers then combine outputs
    rmat=a(:,:,1); % segment image by red colour layer
    grmat=graythresh(rmat); % calculate a suitable threshold for converting image to binary
    brmat=imbinarize(rmat,grmat); % convert segmented image to binary
    gmat=a(:,:,2); % segment image by green colour layer
    ggmat=graythresh(gmat);
    bgmat=imbinarize(gmat,ggmat);
    bmat=a(:,:,3); % segment image by blue colour layer
    gbmat=graythresh(bmat);

```

```

bbmat=imbinarize(bmat,gbmat);
acomb=brmat|bgmat|bbmat;

%% % get inner and outer boundary of rind
ainner=imclearborder(acomb); % remove all regions except the pith region
ainner=bwareafilt(ainner,1);
aoutter=acomb; % make copy of binary image
aoutter(ainner)=0; % remove all regions except the outter rind boundary
aoutter=bwareaopen(aoutter,5000);
aoutter=imcomplement(aoutter); % interchange the black and white regions in the image
aoutter=bwareafilt(aoutter,1);
arind=aoutter&~ainner; % combine the outter boundary and pith mask to obtain section's rind

%% % get coordinates of boundaries
iboundary=bwboundaries(ainner); % trace boundary of pith region
[~,si] = sort( cellfun( @length, iboundary ), 'descend'); % sort obtained cell array of boundaries
from largest to smallest using matrix dimension
iboundary=iboundary(si); % sort boundaries from largest to smallest using above order
icoord=iboundary{1}; % obtain coordinates of pith boundary
xi=icoord(:,2); % x-coordinates of pith boundary
yi=icoord(:,1); % y-coordinates of pith boundary
oboundary=bwboundaries(aoutter); % trace outter boundary of rind
occoord=oboundary{1};
xo=occoord(:,2);
yo=occoord(:,1);
uiwcoord = unique(icoord(:,1:2),'rows','stable'); % take out repeated coordintes from pith
boundary coordinates
uowcoord = unique(occoord(:,1:2),'rows','stable'); % take out repeated coordintes from outter rind
boundary coordinates
uxi=uiwcoord(:,2); % new x-coordinates of pith boundary
uyi=uiwcoord(:,1); % new y-coordinates of pith boundary
si=boundary(uxi,uyi); % extract spline from pith boundary coordinates

```

```

xi=uxi(si); % x-coordinates of extracted pith spline
yi=uyi(si); % y-coordinates of extracted pith spline
isp=[yi,xi]; % combined x and y spline coordinates for pith boundary
uxo=uowcoord(:,2);
uyo=uowcoord(:,1);
so=boundary(uxo,uyo); % extract spline from rind outer boundary coordinates
xo=uxo(so);
yo=uyo(so);
osp=[yo,xo]; % combined x and y spline coordinates for rind outer boundary

% % convert pixel coordinates to mm
s=1/813;
Ri=imref2d(size(ainner),s,s);
for i=1:1:length(isp)
    [ps(i,2),ps(i,1)] = intrinsicToWorld(Ri,isp(i,2),isp(i,1));
end
Ro=imref2d(size(aouter),s,s);
for i=1:1:length(osp)
    [rs(i,2),rs(i,1)] = intrinsicToWorld(Ro,osp(i,2),osp(i,1));
end

% % extract spline from traced boundaries
rsx=rs(:,2); % x-coordinates of rind spline in mm
rsy=rs(:,1); % y-coordinates of rind spline in mm
psx=ps(:,2); % x-coordinates of pith spline in mm
psy=ps(:,1); % y-coordinates of pith spline in mm
ospl=length(osp); % number of rind spline coordinates
rsl=length(rs); % number of rind spline coordinates after conversion to mm
rsxx=rsl-ospl; % check to make sure number of converted coordinates are similar to original
rsr=rsl-(rsxx-1); % check to see if conversion increases coordinates
if rsxx~=0
    rs(rsr:end,:)=[]; % delete extra coordinates created from conversion

```

```

end
ispl=length(isp);
psl=length(ps);
psxx=psl-ispl;
psr=psl-(psxx-1);
if psxx~=0
    ps(psr:end,:)=[];
end
rsx=rs(:,2); % final x-coordinates of rind spline in mm
rsy=rs(:,1); % final y-coordinates of rind spline in mm
psx=ps(:,2); % final x-coordinates of pith spline in mm
psy=ps(:,1); % final y-coordinates of pith spline in mm
% subplot(1,3,3); % display plot in same window as original imported image
axis('on') % display axis on plot
plot(rsx,rsy,psx,psy) % plot rind splines
set(gca,'YDir','reverse'); % reverse y-axis order to get correct orientation of splines

%% find major and minor diameter
C=regionprops(aouter,'Centroid'); % find the centroid of the rind boundary
Cxy=cat(1,C.Centroid); % convert the centroid obtained into a matrix
Cx=Cxy(:,1); % x-coordinate of the centroid
Cy=Cxy(:,2); % y-coordinate of the centroid
[xc,yc]=intrinsicToWorld(Ri,Cx,Cy); % convert centroid coordinates to mm
hold on
plot(xc,yc,'+'); % plot centroid coordinates
Cx=int16(Cx); % convert x coordinate of cenroid to whole number
Cy=int16(Cy); % convert y coordinate of cenroid to whole number
xcl=aouter(:,Cx); % extract vertical column from outter boundary matrix using centroid x-
coordinate
ycl=aouter(Cy,:); % extract horizontal row from outter boundary matrix using centroid y-coordinate
xc_f=find(xcl,1,'first'); % find top coordinate of vertical centre line
xc_l=find(xcl,1,'last'); % find bottom coordinate of vertical centre line

```

```

yc_f=find(ycl,1,'first'); % find first(left) coordinate of horizontal centre line
yc_l=find(ycl,1,'last'); % find last (right) coordinate of horizontal centre line
[xc_t,xc_b]=intrinsicToWorld(Ri,xc_f,xc_l);
[yc_le,yc_r]=intrinsicToWorld(Ri,yc_f,yc_l);
Major_D=xc_b-xc_t; % obtain major diameter
Minor_D=yc_r-yc_le; % obtain minor diameter

%% find the rind thickness of the sample
[dist,S]=pdist2(ps,rs,'euclidean','Smallest',1); % find the shortest pairwise distance between
coordinates of the inner and outer boundary and their indices
rthickness=mean(dist); % calculate the mean of the smallest distances to obtain rind thickness
rt_ips=ps(S,:); % using the indices obtained identify the inner boundary coordinates corresponding
to the shortest distance from the outer boundary
rt_xi=rt_ips(:,2); % x-coordinate of shortest distance
rt_yi=rt_ips(:,1); % y-coordinate of shortest distance

%%% write rind splines
spline = ps; %set inner or outer boundary
splinee = rs; %set inner or outer boundary
filename = sprintf('%s.py',basefilename);
%start a new text file
fileID = fopen(filename,'w');
fprintf(fileID,'from sketch import *\n\n'); %'\n' means go to the next line
fprintf(fileID,'mdb.models["Model-1"].ConstrainedSketch(name="__profile__",
sheetSize=200.0)\n'); %print header information
fprintf(fileID,'mdb.models["Model-1"].sketches["__profile__"].Spline(points=(\n\t');
for i = 1:1:size(spline,1)
    formatSpec = '%4.4f, %4.4f, ';
    fprintf(fileID,formatSpec,spline(i,1),spline(i,2));
end %run through each row and print it to the file
formatSpec = '%4.4f, %4.4f\n'; %re-print first data point to close the spline

```

```

fprintf(fileID,formatSpec,spline(1,1),spline(1,2));
fprintf(fileID,'\t)\n'); %print footer information
fprintf(fileID,'mdb.models["Model-1"].sketches["__profile__"].Spline(points=(\n\t');
for i = 1:size(splinee,1)
    formatSpec = '%4.4f, %4.4f, ';
    fprintf(fileID,formatSpec,splinee(i,1),splinee(i,2));
end %run through each row and print it to the file

formatSpec = '%4.4f, %4.4f)\n';
fprintf(fileID,formatSpec,splinee(1,1),splinee(1,2)); %re-print first data point to close the spline
fprintf(fileID,'\t)\n');
fprintf(fileID,'mdb.models["Model-1"].sketches.changeKey(fromName="__profile__",
toName="rindsplines")\n'); %print footer information
path=strcat('C:\Users\odun3492\Documents\U
Drive\Modeling\fns\splines\w\test\saveall\',basefilename); % insert address of folder where you
intend to save plots
saveas(gcf,path)
save(sprintf('%s.mat',basefilename),'Major_D','Minor_D','rthickness') % this saves in current
matlab folder
close all
end

```